Sedimentary organic carbon dynamics in a glaciated Arctic fjord: tracing contributions of terrestrial and marine sources in the context of Atlantification over recent centuries

Dahae Kim[a], Jung-Hyun Kim[a,*], Youngkyu Ahn[a], Matthias Forwick[b], Seung-Il Nam[a]

[a]Korea Polar Research Institute, 26 Songdomirae-ro, Yeonsu-gu, Incheon 21990, South Korea

[b]UiT The Arctic University of Norway, Department of Geosciences, NO-9037 Tromsø, Norway

***Correspondence:**

Jung-Hyun Kim (jhkim123@kopri.re.kr)

Submitted to Biogeosciences

Abstract

In this study, we investigated sedimentary organic carbon (OC) dynamics in Kongsfjorden, Svalbard, using three multicores collected during the HH22 and HH23 cruises aboard the RV *Helmer Hanssen* in 2022 and 2023. We assessed the relative contributions of petrogenic, soil-derived, plant-derived, and marine OC by applying a four-source apportionment approach based on $\Delta^{14}C_{org}$, $\delta^{13}C_{org}$, and lignin parameters, including the $(Ad/Al)_v$ ratio and lignin phenol concentrations, with Monte Carlo (MC) analysis. Age-depth models based on ^{210}Pb and ^{226}Ra data were used to evaluate temporal variations in the accumulation rates (ARs) of sedimentary OC. Our results revealed a marked increase in marine OC ARs over the past decades, closely linked to enhanced Atlantic Water (AW) inflow. The increasing AW influence in Arctic fjords observed in our record points to the potential for continued Atlantification under Arctic warming, as retreating sea ice and glaciers lower barriers to AW intrusion, enabling deeper and more persistent inflow. By placing this recent AW trend into historical context, our study provides valuable insights into the biogeochemical consequences of ongoing and future climate change in Arctic fjord systems.

Keywords: Svalbard, Kongsfjorden, organic carbon, stable isotopes, radiocarbon isotopes, lignin phenols

1. Introduction

The Arctic region is currently experiencing rapid climate change, with surface air temperatures rising nearly four times faster than the global average since 1979 (Rantanen et al., 2022). This accelerated warming has profound implications for Arctic ecosystems and carbon dynamics (Dahlke et al., 2020; Friedlingstein et al., 2020). Arctic fjords, in particular, are recognized for their high sediment accumulation rates, receiving substantial terrestrial input from glacial meltwater and erosion (Winkelmann and Knies, 2005). As a result, they function as critical hotspots for global organic carbon (OC) burial and serve as high-resolution archives of environmental change (Smith et al., 2015; Bianchi et al., 2020). Given the extreme rates of warming, Arctic fjords are increasingly vulnerable to climate-driven transformations that reflect broader shifts occurring across the Arctic system. While modern observational records provide valuable but temporally constrained insights, sediment cores and other paleoenvironmental archives are essential for reconstructing long-term trends in OC dynamics over the past centuries (Ingrosso et al., 2025).

The high Arctic Svalbard archipelago, a key transitional zone between the North Atlantic and Arctic Oceans, is characterized by widespread glaciation, with approximately 57% of its landmass covered by glaciers (Nuth et al., 2013). A major driver of recent environmental change in this region is the enhanced inflow of warm, saline Atlantic Water (AW) via the West Spitsbergen Current (WSC), which strongly influences the western coast of Spitsbergen, the largest island in the archipelago (De Rovere et al., 2022). This process, termed Atlantification, has intensified over recent decades, accelerating the decline of summer sea ice extent, enhancing tidewater glacier melt, and increasing freshwater discharge into fjords (e.g., Jernas et al., 2018; Krajewska et al., 2020; Skogseth et al., 2020). Kongsfjorden, located on the western coast of Spitsbergen, has emerged as a key site for investigating the impacts of recent Arctic warming due to its dynamic oceanographic regime and sensitivity to AW inflow (e.g., Tesi et al., 2021). Although previous studies have characterized the spatial variability of sedimentary OC in Kongsfjorden using bulk elemental and isotopic parameters (e.g., Winkelmann and Knies, 2005; Kuliński et al., 2014; Kumar et al., 2016) molecular-level assessments of sedimentary OC sources, espically over the past centuries, remain limited.

A recent study by Kim et al. (2023) began addressing this gap by analyzing the sources and composition of surface sedimentary OC across eight Svalbard fjords, including Kongsfjorden. Their findings provided valuable insights into the spatial

patterns of contemporary OC dynamics. However, the study did not address the progressive shifts in OC dynamics linked to Atlantification since the mid-1990s, an era marked by intensified AW intrusion and ecosystem change. These longer-term oceanographic transformations have been well-documented (e.g., Årthun et al., 2012; Polyakov et al., 2017; Lind et al., 2018; Tesi et al., 2021) but are not yet fully integrated into our understanding of sedimentary OC in Svalbard fjords. The lack of long-term observational and historical data on AW inflow in this region highlights the urgent need for sedimentary records to establish baselines and quantify rates of environmental change (e.g., Cottier et al., 2007; Tesi et al., 2021; Jordà-Molina et al., 2023). Such records are invaluable for distinguishing between natural variability and human-induced changes, providing insights into the mechanisms driving environmental changes in Arctic fjords.

Building on the findings of Kim et al. (2023), this study aimed to generate longer-term reconstructed records to fill the current gap in long-term observational and historical data on AW inflow in this region, through the analysis of three multicores collected along a transect from the inner to the outer Kongsfjorden. The primary objectives were to: (1) characterize spatial patterns of sedimentary OC, (2) estimate temporal variations in the relative contributions of sedimentary OC sources over the past centuries, and (3) assess the impact of human-induced climate variability on environmental conditions. To achieve these aims, we applied a multi-proxy approach that integrates bulk geochemical parameters (carbon and nitrogen contents, stable carbon and radiocarbon isotopes), molecular biomarkers (lignin phenols), and sedimentological measurements (bulk dry density, grain size, and surface area). This integrative framework provides critical insights into the coupling between terrestrial and marine systems, and highlights the sensitivity of Arctic fjord environments to both past and ongoing climate change.

2. Regional setting

Kongsfjorden and Krossfjorden form the Kongsfjorden–Krossfjorden fjord system, which opens westward into the Kongsfjordrenna, a submarine glacial trough that incises the continental shelf off northwestern Spitsbergen (Fig. 1; Svendsen et al., 2002). This high-latitude fjord complex spans 78°50′ to 79°30′ N and 11° to 13° E. Kongsfjorden, the southern branch (~20 km long, 4–10 km wide, up to 394 m deep), holds ~29.4 km^3 of water, while Krossfjorden, the northern branch (~30 km long, 3–6 km wide, max depth 374 m), contains ~25 km^3 (Ito and Kudoh, 1997; Svendsen et al., 2002). Kongsfjorden's drainage basin (~1440 km^2) is ~80% glaciated (Pramanik et al., 2020), receiving

substantial freshwater and sediment from five tidewater glaciers (Kongsvegen, Kronebreen, Kongsbreen, Conwaybreen, and Blomstrandbreen) and the Bayelva River (Zhu et al., 2016; McGovern et al., 2022).

The absence of a sill at the mouth of Kongfjorden allows intrusions of warm (~6°C), saline, nutrient-rich AW (Svendsen et al., 2002; Cantoni et al., 2020). These intrusions, driven by variability in the WSC and wind-induced shelf processes, typically enter at intermediate depths (~100–200 m), increasing subsurface temperatures and salinities and altering hydrographic structure (Svendsen et al., 2002; Tverberg et al., 2019; De Rovere et al., 2022). This weakens stratification, enhances vertical mixing, and impacts sea ice dynamics, glacier melting, and biogeochemical cycles. When occurring during the productive season, AW intrusions can also stimulate primary productivity by delivering nutrients to the euphotic zone. During periods of weak AW advection, colder, fresher Arctic Water from the East Spitsbergen Current (ESC) dominates, strengthening stratification and promoting a more Arctic-like regime.

In addition to oceanic forcing, glacial meltwater strongly influences fjord hydrography and ecology. Meltwater from tidewater glaciers transports large sediment loads, generating turbid plumes that reduce light penetration and suppress primary productivity, particularly near glacier fronts (Ito and Kudoh, 1997; Svendsen et al., 2002). These inputs also deliver terrestrial organic carbon (OC), including petrogenic OC from eroded bedrock and aged OC from soils. Surface runoff from glacial forefields and surrounding catchments further contributes to sediment and OC input. These effects are sustained by the fjord's long water residence time and limited exchange with the open ocean, which support internal circulation and persistent stratification (Svendsen et al., 2002; Cottier et al., 2005; Tverberg et al., 2019).

3. Material and methods

3.1 Sample collection

Four surface sediment samples were collected from Kongsfjorden and Krossfjorden during the RV *Helmer Hanssen* cruise (HH23) in 2023 (Fig. 1). Three multicores were recovered from Kongsfjorden, Svalbard, at water depths of 81 m (core HH23-1058MUC, hereafter 1058MUC; 45 cm long), 339 m (core HH22-1161MUC, hereafter 1161MUC; 44 cm long), and 323 m (core HH22-1159MUC, hereafter 1159MUC; 40 cm long) during the RV *Helmer Hanssen* cruises (HH22 and HH23) in 2022 and 2023 (Fig. 1). The cores were retrieved using a multi-corer (KC Denmark model 72.000, with 6 core liners; 11 cm

outer diameter; 10.5 cm inner diameter, and 0.8 m length each). The multicores were sectioned onboard at 0.5 cm intervals down to 2 cm depth, and at 1 cm intervals thereafter and stored at –20°C. Subsequently, the samples were freeze-dried for further analysis.

3.2 Sedimentological analysis

To characterize sedimentary properties associated with OC transport and deposition, we analyzed water content, dry bulk density, grain size distribution, , and specific surface area. Water content was calculated by determining the weight loss of wet bulk samples after freeze-drying. The dry bulk density of homogenized subsamples was measured using an AccuPyc II 1345 pycnometer (Micromeritics, Georgia, USA) at the Korea Polar Research Institute (KOPRI). The average of three measurements was used for grain density calculations to ensure precision, with an analytical error of less than 0.0032 cm^3 observed when employing the 1 cm^3 chamber. Grain size distribution followed the methodology outlined by Ahn et al. (2024). Approximately 130 mg of freeze-dried, unground subsamples were treated with 5 mL of 35% H_2O_2 to oxidize organic matter. A Mastersizer 3000 laser particle size analyzer (Malvern Panalytical B.V., UK) was used for grain size analysis of bulk sediments at KOPRI. Analytical precision was determined as follows: D(10): 37.5 ± 0.3 μm, D(50): 71.4 ± 0.2 μm, D(90): 104.0 ± 0.0 μm. Specific surface area (SA) measurements were conducted following the method described by Kim et al. (2022). Freeze-dried, unground subsamples were first heated at 350°C to remove organic matter and then cooled gradually over 12 hours to room temperature. Prior to analysis, the samples were degassed at 200°C for 2 hours under a constant flow of N_2 gas using a Micromeritics FlowPrep 060 Sample Degas System at the Korea Basic Science Institute (KBSI, Jeonju Center). Specific SA was measured with N_2 gas as the adsorbate in a He atmosphere, with an analytical precision within ± 9%. Instrument performance was verified using Carbon Black (21.0 ± 0.75 m^2/g; ISO 9277:2010), a certified reference material provided by Micromeritics.

3.3 Radioisotope analysis

To establish sediment chronology and determine sedimentation rates, freeze-dried and ground subsamples (~5 g) were analyzed for ^{210}Pb and ^{226}Ra activities using gamma spectrometry with a well-type High-Purity Germanium (HPGe) detector at KBSI. The analytical uncertainties averaged 9.6 ± 2.0 mBq/g for ^{210}Pb and 2.7 ± 4.1 mBq/g for ^{226}Ra. Excess ^{210}Pb ($^{210}Pb_{ex}$) activities were calculated by subtracting the ^{226}Ra activity from the

total ^{210}Pb ($^{210}Pb_{tot}$) activity, following the approach described by Appleby (1998). The apparent sedimentation rate (cm/yr) was calculated from $^{210}Pb_{ex}$ with the constant rate of supply (CRS) model (cf. Appleby and Oldfield, 1978) with the following equation:

$$\text{Apparent sedimentation rate} = -\lambda / b \text{ (cm/yr)} \quad (1)$$

where λ is the radioisotope decay constant for ^{210}Pb (0.03114 per year), and b is the slope of the regression line.

3.4 Bulk elemental and carbon isotope analysis

To determine the content and isotopic composition of OC and to infer its sources, we conducted bulk elemental and carbon isotope analyses, including $\delta^{13}C_{org}$ and $\Delta^{14}C_{org}$. The bulk elemental and carbon isotopic composition were determined using the procedure based on Kim et al. (2023). In brief, total nitrogen (N_{tot}) and total organic carbon (TOC) contents, as well as carbon isotopic compositions ($\delta^{13}C_{org}$), were analyzed using an elemental analyzer (Thermo Electron Corporation Flash EA 2000, Thermo Fisher Scientific, Germany) connected to an isotope ratio mass spectrometer (Finnigan Delta Plus, Thermo Fisher Scientific, Germany). TOC and $\delta^{13}C_{org}$ were measured on decalcified samples using 1 M HCl for 24 hours. The $\delta^{13}C_{org}$ values were expressed in delta notation (‰) relative to the Vienna Pee Dee Belemnite (VPDB) standard. The analytical precision was within 0.5 wt. % for carbon, 0.5 wt. % for nitrogen, and 0.5‰ for $\delta^{13}C_{org}$.

Sediment samples were pretreated with HCl and NaOH to remove carbonates and humic acids, followed by drying at 60°C. The alkali-insoluble fraction was combusted at 900°C in sealed ampoules with CuO to produce CO_2, which was then purified and converted to graphite following the mehtod of Vogel et al. (1984). Radiocarbon ($^{14}C/^{13}C$) measurements were performed using accelerator mass spectrometry (AMS) at the Center for Applied Isotope Studies (CAIS), University of Georgia, USA. The radiocarbon results were presented in delta notation ($\Delta^{14}C_{org}$, ‰), as defined by Stuiver and Polach (1977).

3.5 Lignin phenol analysis

To trace terrestrial OC inputs, particularly those derived from vascular plants, we analyzed lignin phenols using CuO oxidation followed by gas chromatography-mass

spectrometry. CuO oxidation and subsequent analyses were performed following the procedure described by Kim et al. (2023). In brief, homogenized subsamples (~400 mg) were subjected to alkaline CuO oxidation in the presence of cupric oxide and ammonium iron (II) sulfate hexahydrate. This process was conducted using a Microwave Digestion System (MARS 6 microwave, CEM Corporation, USA) at 150°C for 1.5 hours after adding N_2-purged NaOH solution. After oxidation, a known amount of internal standard (ethyl vanillin) was added to the CuO oxidation products. The resulting products were analyzed at KOPRI using an Agilent 7890B gas chromatograph (GC) coupled to a 5977B Series Mass Selective Detector (MSD) (Agilent Technologies, Santa Clara, CA, USA). Analyses were conducted in single ion monitoring (SIM) mode with a DB1-MS capillary column (30 m × 0.25 mm, 0.25 μm, Agilent J&W). The analytical uncertainty for lignin phenols concentrations, determined through replicate measurements of the same sediment samples, was typically less than 10%. Calibration was performed using commercially available standards.

3.6 Accumulation rates

The accumulation rates (AR) of each OC source in the sediment cores were calculated to investigate OC fluxes over recent timescales. Wet bulk density (WBD) and porosity (PO) were determined using the water content and dry bulk density of the samples, as described by Hamilton (1971). The AR was calculated based on the sedimentation rate (SR), WBD, and PO of each sample, as follows (cf. Gealy, 1971):

$$AR\ \left(\frac{g/cm^2}{yr}\right) = \mathrm{SR} \times \left[WBD - 1.025 \times \left(\frac{PO}{100}\right)\right] \quad (2)$$

As the next step, the ARs of bulk OC were calculated using Equation 2, as follows (cf. Nam, 1997):

$$\text{Bulk OC AR} = (\text{TOC of sediment sample}/100) \times \text{AR} \quad (3)$$

The ARs of petrogenic, soil-derived, plant-derived, and marine OC were calculated from bulk OC AR using Equation 3, as follows:

AR of each OC source = (each OC source fraction/100) × bulk OC AR (4)

4. Results

4.1 Sediment properties

The depth profiles of water content, dry bulk density, grain size distribution, mean grain size, and specific surface area (SA) for the three cores are shown in Fig. 2. Water content displayed distinct trends across the cores. The highest water content was observed at the outermost site (core 1159MUC), ranging from 30.3% to 47.5%, with an average of 38.5 ± 3.2%. At the middle site (core 1161MUC), water content ranged from 31.7% to 42.2%, with an average of 35.3 ± 2.2%. The innermost site (core 1058MUC) exhibited the lowest range, from 19.7% to 32.6%, with an average of 27.9 ± 2.3%.

Dry bulk density measurements showed a decreasing trend from the innermost to the outermost core. Core 1058MUC had a dry bulk density ranging from 2.74 g/cc to 2.77 g/cc, for core 1161MUC, the range was 2.68 g/cc to 2.80 g/cc. For core 1159MUC, the range was 2.60 g/cc to 2.69 g/cc.

In general, silt content was predominant in all three cores, with the highest average observed at the innermost site (core 1058MUC), where it reached 90 ± 2%. Mean grain sizes varied across the sites, with the innermost site (core 1058MUC) showing the largest grain sizes, ranging from 8.8 μm to 13.3 μm. The middle site (core 1161MUC) exhibited a slightly smaller range, from 7.9 μm to 13.0 μm, while the outermost site (core 1159MUC) ranged from 8.3 μm to 11.0 μm.

Mineral-specific surface area (SA) values decreased with distance from the inner fjord site. Core 1058MUC showed values between 10.0 m^2/g and 16.5 m^2/g, core 1161MUC ranged from 8.6 m^2/g to 13.9 m^2/g, and core 1159MUC exhibited the lowest range, from 8.3 m^2/g to 11.0 m^2/g.

4.2 ^{210}Pb geochronology

The depth profiles of total ^{210}Pb ($^{210}Pb_{tot}$) and excess ^{210}Pb ($^{210}Pb_{ex}$) activities for the two cores are displayed in Fig. 3. A sediment core collected in 2000 by Zaborska et al. (2006) from inner Kongsfjorden, near the core 1058MUC site, showed a sedimentation rate (SR) of ~0.15 cm/yr based on ^{210}Pb dating. However, core 1058MUC was excluded from ^{210}Pb analysis due to the potential for high sedimentation rates and intense sediment mixing near glacier fronts, which can disrupt sediment stratigraphy and reduce the

reliability of age-depth models (e.g., López et al., 2020; Schirone et al., 2022). Core 1161MUC exhibited $^{210}Pb_{tot}$ values ranging from 89.3 mBq/g to 233.0 mBq/g, while core 1159MUC showed a broader range from 22.1 mBq/g to 246.6 mBq/g. For $^{210}Pb_{ex}$, core 1161MUC had values between 59.6 mBq/g and 207.2 mBq/g, while core 1159MUC displayed a range from 9.3 mBq/g to 216.0 mBq/g. Based on these profiles, the sedimentation rate (SR) was calculated as 0.36 cm/yr at the middle site (core 1161MUC) and 0.12 cm/yr at the outermost site (core 1159MUC).

4.3 Bulk elemental and carbon isotopic compositions

The depth profiles of bulk elemental and carbon isotope parameters for the three sediment cores are shown in Fig. 4. The TOC content showed clear trends depending on the core location. Core 1058MUC had values ranging from 0.2 to 0.4 wt.% (average 0.3 ± 0.0 wt.%), while core 1161MUC ranged from 0.9 to 1.5 wt.% (average 1.2 ± 0.1 wt.%), and core 1159MUC exhibited the highest values, ranging from 1.9 to 2.5 wt.% (average 2.2 ± 0.2 wt.%). A similar pattern was observed for total nitrogen (N_{tot}) content: core 1058MUC ranged from 0.01 to 0.05 wt.%, core 1161MUC ranged from 0.08 to 0.13 wt.%, and core 1159MUC exhibited values from 0.22 to 0.26 wt.%. Previous studies conducted in various Svalbard fjords showed that surface sediments contained a substantial proportion of inorganic nitrogen, up to 70% of the N_{tot} content (Fig. S1A), with a significant correlation between inorganic nitrogen and clay mineral content (Schubert and Calvert, 2001; Winkelmann and Knies, 2005; Knies et al., 2007; Knies and Martinez, 2009; Kumar et al., 2016; Kim et al., 2023). Consistent with the strong linear relationship (R^2 = 0.89, Fig. S1A) between N_{tot} and organic nitrogen (N_{org}) reported in surface sediments from multiple Svalbard fjords (Kim et al., 2023), our subdataset from Kongsfjorden and Krossfjorden showed an even stronger correlation (R^2 = 0.96, Fig. S1B). This high degree of correlation allowed us to estimate N_{org} from N_{tot} using the derived regression equation: $N_{org} = 0.7863 \times N_{tot} - 0.0096$. Based on this method, the estimated N_{org} content ranged from 0.01 to 0.03 wt.% (average 0.01 ± 0.00 wt.%) for core 1058MUC, from 0.05 to 0.09 wt.% (average 0.07 ± 0.01 wt.%) for core 1161MUC, and from 0.14 to 0.17 wt.% (average 0.15 ± 0.01 wt.%) for core 1159MUC. However, it is important to consider that inorganic nitrogen content can vary with sediment type and depth, which may influence the accuracy of the estimated N_{org}. Therefore, although this regression-based method provided a practical approximation, caution was warranted

when interpreting the estimated N_{org} values, particularly in sediments with heterogeneous stratigraphy or mineral composition.

The molar N_{tot}/TOC ratios were lowest in core 1058MUC, varying from 0.04 to 0.12 (average 0.06 ± 0.02), followed by core1161MUC, ranging from 0.06 to 0.11 (average 0.07 ± 0.01), and core 1159MUC with values between 0.08 and 0.11 (average 0.09 ± 0.01). The N_{org}/TOC ratios showed a similar pattern, being lower than the corresponding N_{tot}/TOC ratios, with core 1058MUC ranging from 0.03 to 0.08, core 1161MUC ranging from 0.04 to 0.07, and core1159MUC ranging from 0.05 to 0.07.

The $\delta^{13}C_{org}$ values exhibited a distinct offshore-increasing trend. Core 1058MUC displayed values ranging from –24.6‰ to –22.5‰ (average –23.5 ± 0.5 ‰). Core 1161MUC values ranged from –23.9‰ to –22.3‰ (average –23.2 ± 0.3 ‰), while core 1159MUC showed the most enriched values, ranging from –23.5‰ to –22.4‰ (average –22.7 ± 0.3 ‰). A similar pattern was observed for $\Delta^{14}C_{org}$ values, which increased from the innermost to the outermost site. Core 1058MUC ranged from –839.2‰ to –743.5‰ (average –793.9 ± 31.1 ‰). Core 1161MUC exhibited values from –555.9‰ to –405.7‰ (average –504.9 ± 44.0 ‰), and core 1159MUC showed values between –469.3‰ and –396.7‰ (average –433.5 ± 21.7 ‰).

4.4 Lignin phenol compositions

The depth profiles of the products of alkaline CuO oxidation for the three sediment cores are presented in Fig. 5. Total lignin phenol concentrations, which represent the sum of eight lignin-derived monomeric phenols (vanillyl (V), syringyl (S), and cinnamyl (C) units), normalized to TOC, showed clear variation with depth and location. Core 1058MUC had the highest total lignin phenol concentrations, ranging from 0.24 to 0.66 mg/gOC (average 0.40 ± 0.12 mg/gOC). Cores 1161MUC and 1159MUC showed similar concentrations, with overlapping ranges and comparable average values. Specifically, core 1161MUC ranged from 0.07 to 0.19 mg/gOC (average 0.14 ± 0.04 mg/gOC), and core 1159MUC ranged from 0.06 to 0.22 mg/gOC (average 0.12 ± 0.04 mg/gOC), indicating no significant difference between the two sites.

The S/V and C/V ratios, which reflect the type of organic material derived from vascular plants, followed a consistent pattern, with higher values at the innermost site. For core 1058MUC, the S/V ratio ranged from 0.01 to 0.63, and the C/V ratio ranged from 0.00 to 0.55. At the middle site (core 1161MUC), the S/V ratio ranged from 0.07 to

0.36, and the C/V ratio from 0.00 to 0.25, both decreasing relative to the inner site. Core 1159MUC showed S/V values between 0.13 and 0.49 and C/V values from 0.14 to 0.41, which were higher than those at the middle site but still lower than those at the innermost site.

The 3,5-Bd/V ratios, indicative of the extent of lignin degradation, varied significantly among the sites. Core 1058MUC showed values from 0.06 to 0.55, while core 1161MUC exhibited a broader range from 0.47 to 2.59. Core 1159MUC had the highest 3,5-Bd/V ratios, ranging from 0.59 to 2.46, indicating more extensive oxidation of lignin-derived compounds at the outer site. Similarly, the (Ad/Al)v ratios, which represent the degree of oxidative alteration of lignin side chains, exhibited a comparable trend. Core 1058MUC showed values between 0.22 and 0.89, while core 1161MUC ranged from 0.40 to 1.60. The highest values were observed in core 1159MUC, ranging from 0.37 to 1.74, further supporting the trend of increased lignin degradation in sediments toward the outer fjord.

5. Discussion

5.1 Grain size end-member modelling

Grain-size end-member (EM) modeling identifies representative patterns within a sediment's grain-size distribution, allowing for inferences about the influence of depositional processes based on variations in the relative abundances of each EM (van Hateren et al., 2018). Following the approach used by Ahn et al. (2024) in Wijdefjorden, northern Svalbard, grain-size EM modeling was performed to analyze variations in the grain-size distribution of the three cores investigated in this study. Two candidate Q values were identified (Fig. S2), with R^2 values exceeding 0.6 for each core (Fig. S3). The optimal Q value was selected by comparing the extracted EMs with the analyzed grain-size distribution curves (Fig. S4). From the three cores, a total of eight EMs were extracted (Fig. S5) and subsequently classified into four primary EM groups (Fig. 6A). EM1 primarily consisted of fine-grained sediment (very fine to medium silt, 2–16 μm), with EM1b having a relatively coarser-dominant mode (primary mode: 9.3–15.5 μm, very fine to medium silt: 54.3–59.7%) compared to EM1a (primary mode: 8.2–9.3 μm, very fine to medium silt: 62.2–66.8%). In contrast, EM2 was dominated by coarser grains (medium to very coarse silt, 8–63 μm, 66.4%), with a coarse primary mode of 29.3 μm. Notably, EM3 exhibited a wide range of grain sizes, including both fine and coarse

particles, with modes at 9.3 and 81.2 μm.

The EM results revealed that EM1a and EM1b, primarily consisting of the finest grains, were present in all three sediment cores (Fig. 6B). These fine-grained sediments are generally deposited through size-dependent settling of suspended particles from meltwater and/or glaciofluvial discharge (Ó Cofaigh and Dowdeswell, 2001; Forwick and Vorren, 2009; Elverhøi et al., 1980). The flocculation in seawater further promotes their settling (Meslard et al., 2018), facilitating the transport of both EM1a and EM1b from the inner to the outer fjord. The distinction between EM1a and EM1b deposition is influenced by the strength of meltwater discharge, with stronger discharge suspending and transporting relatively coarser particles found in EM1b (Ahn et al., 2024). In contrast, coarse-grained sediments, primarily represented by EM2, were observed only at the innermost site (core 1058MUC), situated closest to the glacier front (Fig. 6B). This area is likely influenced by bottom currents driven by subglacial meltwater outflow (Meslard et al., 2018; Torsvik et al., 2019). The scarcity of fine particles in EM2 reflects the winnowing effect of these currents, which preferentially remove finer material and leave behind coarser sediments (Vorren et al., 1984). Such glacially influenced environments are typically characterized by poorly sorted sediments (Hass, 2002), and strong bottom currents (Ahn et al., 2024) that promote coarse-grained deposition near glacier fronts. On the other hand, EM3 contains both fine and coarse particles, with a coarse mode reaching 81.2 μm, significantly larger than the principal mode of EM2. EM3 was found exclusively in the middle core (1161MUC), located at the central site of Kongsfjorden. This distribution corresponds to the presence of multiple sediment sources in the mid-fjord region, where fluvial inputs from land-terminating glaciers, such as the Bayelva River near Ny-Ålesund, deliver mixed sediments and terrestrial OC (D'Angelo et al., 2018; Husum et al., 2019).

5.2 Source of sedimentary organic carbon: bulk parameters

The TOC values of the three sediment cores varied significantly along Kongsfjorden, with the innermost core (1058MUC) having the lowest TOC (average 0.3 ± 0.0 wt.%), and the outermost core (1159MUC) the highest (average 2.2 ± 0.2 wt.%) (Fig. 4). This variation was also reflected in the TOC/SA ratio (Figs. 7A-7B), which indicates OC loading and serves as a measure of OC preservation efficiency (Keil et al., 1994; Mayer et al., 1994; Stein et al., 2004; Zonneveld et al., 1997). Values between 0.4

and 1.0 suggest a balance between OC supply and degradation (Keil et al., 1997). However, values below 0.4 are observed in the innermost core. In Kongsfjorden, D'Angelo et al. (2018) reported that lithogenic material accounted for the dominant sediment fraction (64–78%), and Svendsen et al. (2002) highlighted significant deposition of mineral material in the inner fjord. Therefore, the lower OC loading in the innermost core (1058MUC) is likely attributed to the deposition of coarse-grained terrestrial minerals (see Fig. 6B) that dilute the OC content. In contrast, higher OC loading in the middle and outer cores, with values greater than 1.0, suggests enhanced OC preservation efficiency, likely due to adsorption onto fine-grained minerals (see Fig. 6B) that reduce degradation (Keil et al., 1994; Mayer, 1994; Blair and Aller, 2012).

Similar to TOC, both N_{tot} and N_{org} values were highest in the outermost core (1159MUC) compared to the middle (1161MUC) and innermost (1058MUC) cores (Fig. 7C; see also Fig. 4). TOC and N (both N_{tot} and N_{org}) contents in all three cores largely overlapped with those reported for surface sediments from Kongsfjorden and Krossfjorden (Kim et al., 2023 and references therein). In contrast, small drifted ice samples containing ice-rafted debris (IRD) from the fjords had lower TOC (0.1 ± 0.0 wt.%) and N_{tot} (0.04 ± 0.01 wt.%) contents, whereas coal samples from Kongsfjorden exhibited significantly higher values (TOC: 50.8 ± 11.1 wt.%; N_{tot}: 0.86 ± 0.04 wt.%). The N_{tot}/TOC and N_{org}/TOC ratios were also highest in the outermost core (Fig. 7D; see also Fig. 4). Additionally, the $\delta^{13}C_{org}$ values were more enriched in the outermost core (Fig. 7D; see also Fig. 4), suggesting an increased contribution of marine OC to sedimentary OC toward the outer fjord. Notably, the $\delta^{13}C_{org}$ values from all three cores fell within the range observed in the small drifted ice containing IRD samples (–21.8 ± 2.1 ‰), coal samples (–24.4 ± 1.6 ‰), and surface sediments from Kongsfjorden (–23.0 ± 0.7 ‰). However, the $\delta^{13}C_{org}$ values of most surface sediments and small drifted ice containing IRD samples from Krossfjorden were higher than those from Kongsfjorden, generally falling outside the range observed in all three cores. This difference may be associated with the Quaternary marine deposits exposed in Krossfjorden (Fig. S6, Dallmann and Elvevold, 2015), which could supply older, ^{13}C-enriched marine-derived OC. These observations suggest that the contribution of Krossfjorden to sedimentary OC in all three cores was minimal. The $\Delta^{14}C_{org}$ values of the innermost core (1058MUC) were more depleted than those of the other two cores (Figs. 7E-7F). Similarly, small drifted ice containing IRD and surface sediment samples collected near the marine-terminating glacier front in Kongsfjorden exhibited similarly depleted values. Notably, the $\Delta^{14}C_{org}$

values of the other two cores fell between those of the glacier-front samples and those from the outer fjord. These results align with Kim et al. (2023), who suggested that the significant depletion of $\Delta^{14}C_{org}$ in the surface sediments of Svalbard fjords indicates that recently fixed terrestrial and marine OC alone cannot account for the sedimentary OC. Instead, a substantial amount of old OC, likely from petrogenic and soil-derived sources, contributes to the sedimentary OC in Kongsfjorden.

The relationship between TOC and mean grain size showed no clear correlation, with the sediments predominantly consisting of silt fractions (Fig. S7A). Similarly, TOC content did not exhibit a distinct relationship with sediment sorting values (Fig. S7B). The sediments were generally poorly sorted, with high silt content, a characteristic feature of glacial environments, where deposits are typically incompletely sorted due to the non-selective nature of glacial transport (Singh et al., 2019). The consistently poor sorting observed across all morphological zones, along with the absence of correlation between TOC and mean grain size, suggests a glacier-fed depositional system influenced by variable hydrodynamic conditions driven by meltwater discharge. At the middle site, the presence of EM3 indicates a contribution of terrestrial material via fluvial processes. However, the proportion of EM3 was relatively low (18.2 ± 14.9%) compared to EM1a and EM1b (81.8 ± 14.9%; Fig. 6), suggesting that glacial meltwater remains the dominant sediment delivery mechanism at this site, with only a minor influence from surface runoff processes. Overall, the sedimentary characteristics of Kongsfjorden indicate a fjord environment significantly influenced by glacial input. The repeated cycles of glacial advance and retreat have resulted in the accumulation of sediments with varied grain sizes and sorting patterns, reflecting the dynamic and complex interplay between terrestrial and marine OC processes within this glaciated fjord system.

5.3 Source of sedimentary organic carbon: lignin phenol parameters

In a previous study conducted in Svalbard fjords, Kim et al. (2023) defined two OC components (petrogenic OC and biogenic OC) to identify the source of ^{14}C-depleted OC in sedimentary OC. To further investigate the contributions of biogenic OC sources to Kongsfjorden, we analyzed lignin phenols obtained through alkaline CuO oxidation. Lignin phenols serve as valuable terrestrial biomarkers because they are exclusively synthesized by terrestrial higher plants (Hedges and Mann, 1979; Goñi et al., 2005). The ratios of S/V and C/V are used to evaluate the relative contributions of four components:

474 non-woody angiosperms, woody angiosperms, non-woody gymnosperms, and woody
475 gymnosperms (Hedges and Mann, 1979; Goñi and Hedges, 1995). In the three
476 Kongsfjorden cores, lignin phenols primarily consisted of a mixture of non-woody
477 gymnosperm OC with inputs from gymnosperm wood-derived tissues, along with some
478 contributions from non-woody angiosperms, consistent with previous studies (Fig. 8A).
479 The strong gymnosperm signal observed in both surface and downcore sediments, despite
480 the current dominance of angiosperm vegetation in the Svalbard archipelago, suggests a
481 substantial contribution of OC from older terrestrial sources, such as permafrost-stored
482 material. This implies that the terrestrial OC preserved in these sediments likely reflects
483 inputs from past vegetation communities, rather than representing solely contemporary
484 plant cover. Lignin phenol concentrations were highest in the innermost core (1058MUC)
485 compared to the other two cores (Fig. 8B; see also Fig. 5), and fell within the range
486 observed in surface sediments from Svalbard fjords, including Kongsfjorden and
487 Krossfjorden (Figs. S8A and S9A).
488 3,5-Bd is primarily produced during soil degradation processes, leading to its
489 enrichment in soils (e.g., Prahl et al., 1994; Goñi et al., 2000; Houel et al., 2006; Otto and
490 Simpson, 2006). As a result, the 3,5-Bd/V ratio is widely used to assess the extent of
491 lignin degradation and to trace inputs of soil-derived OC to aquatic systems (e.g., Prahl
492 et al., 1994; Goñi et al., 2000; Houel et al., 2006; Otto and Simpson, 2006). Similarly, the
493 (Ad/Al)v ratio reflects lignin oxidation, as the conversion of aldehyde functional groups
494 into acidic phenols through propyl side-chain modification serves as a key indicator of
495 lignin degradation in sedimentary organic matter (e.g., Hedges and Ertel, 1982; Goñi and
496 Hedges, 1992; Otto and Simpson, 2006). (Ad/Al)v ratios below 0.3 typically indicate
497 relatively fresh vascular plant detritus, whereas values exceeding 0.5 are generally
498 associated with extensively altered soils with significantly depleted ^{14}C signatures (e.g.,
499 Hedges and Ertel, 1982; Goñi and Hedges, 1992; Otto and Simpson, 2006). Among the
500 three cores, both 3,5-Bd/V and (Ad/Al)v ratios were lowest in the innermost core
501 (1058MUC) (Figs. 8C and 8D; see also Fig. 5). Notably, coal samples also exhibited
502 relatively low values, averaging 0.48 for the 3,5-Bd/V ratio and 0.49 for the (Ad/Al)v
503 ratio, similar to those of the innermost core (1058MUC). Both the 3,5-Bd/V and (Ad/Al)v
504 ratios were higher in the outermost core (1159MUC) compared to the middle (1161MUC)
505 and innermost (1058MUC) cores, indicating a higher degree of lignin degradation toward
506 the outer fjord. This trend likely reflects cumulative degradation processes occurring
507 during offshore transport rather than differences in terrestrial OC sources alone. Notably,

the inter-site variation was more pronounced for the 3,5-Bd/V ratio than for the (Ad/Al)v ratio.

Previously, Kim et al. (2023) suggested that biogenic OC includes not only recently fixed terrestrial and marine biomass but also pre-aged OC from soils, which can be transported to fjords through glacial erosion and surface runoff. Therefore, we examined the lignin phenol concentrations and (Ad/Al)v ratios of these biogenic OC sources—plant-derived, soil-derived, and marine OC (Fig. S8). Most core sediments exhibited lower lignin phenol concentrations and (Ad/Al)v ratios compared to the average values of soils collected in the Ny-Ålesund and Longyearbyen regions. Thus, the soil values encompass the range observed in all three cores and most surface sediments collected in Svalbard fjords. However, surface sediments from Krossfjorden exhibited distinct (Ad/Al)v ratios and $\delta^{13}C_{org}$ values, which fell outside the soil range. This difference may result from the complex bedrock types present in Svalbard fjords (Fig. S6), which can influence OC characteristics (Kim et al., 2023). These findings suggest that the contribution of Krossfjorden to the sedimentary OC in all three cores was limited.

5.4 Four OC source apportionments

In this study, we adopted the OC source classification concept from the surface sediment study in Svalbard fjords (Kim et al., 2023) and defined four distinct sedimentary OC sources: petrogenic, soil-derived, plant-derived, and marine OC. To estimate the relative proportions of these OC sources, we applied a four-source apportionment approach based on $\Delta^{14}C_{org}$, $\delta^{13}C_{org}$, and lignin parameters such as the (Ad/Al)v ratio and lignin phenol concentrations, using a Monte Carlo (MC) analysis. End-member values for each OC source, as reported in Kim et al. (2023; Table S1), were used in the analysis.

Firstly, similar to the previous study by Kim et al. (2023), the relative proportions of the four OC sources were calculated using Method 1, based on $\Delta^{14}C_{org}$, $\delta^{13}C_{org}$, and the (Ad/Al)v ratio (Fig. 9). The petrogenic OC fraction was highest in core 1058MUC, located at the innermost site, with an average of 79.2 ± 3.4%. This was followed by core 1161MUC (average 44.7 ± 5.7%) and core 1159MUC (average 37.8 ± 5.0%). In constrast, marine OC fractions were highest in core 1159MUC at the outermost site (average 44.0 ± 5.2%), followed by core 1161MUC (average 38.4 ± 7.8%) and core 1058MUC (average 19.0 ± 3.9%).

Secondly, we calculated the relative proportions of the four OC sources using Method 2, which is based on $\Delta^{14}C_{org}$, $\delta^{13}C_{org}$, and lignin phenol concentrations. This

542 method was chosen because previous studies used lignin phenol concentrations for source
543 mixing models, assuming a value of 0 for marine phytoplankton (Tesi et al., 2016;
544 Pempkowiak et al., 2020). To validate this approach, we first applied Method 2 to surface
545 sediments previously investigated by Kim et al. (2023). Overall, the estimated relative
546 contributions of the four OC sources were within a similar range to those reported in the
547 earlier study, and the spatial distribution pattern exhibited similar trends between both
548 approaches (Fig. S10). For the three sediment cores in this study, the results from Method
549 2 also were consistent with those from Method 1. Petrogenic OC fractions were highest
550 in core 1058MUC, located at the innermost site (average 79.2 ± 3.3%), followed by cores
551 1161MUC (average 46.6 ± 4.4%) and 1159MUC (average 40.7 ± 1.7%) (Fig. 9). In
552 contrast, marine OC fractions were greatest in core 1159MUC at the outermost site
553 (average 50.4 ± 4.7%), followed by core 1161MUC (average 42.9 ± 5.2%) and core
554 1058MUC (average 16.5 ± 3.2%). These findings suggest that Method 2 did not
555 significantly alter the trends observed from Method 1. However, it is important to note
556 that some surface sediments from Kongsfjorden and Krossfjorden exhibited (Ad/Al)v
557 ratios outside the range of soil values (Fig. S9B). In contrast, the lignin phenol
558 concentration data were well within the expected range for soils (Fig. S9A). Given this,
559 Method 2 appears to be a more appropriate approach than Method 1 for assessing the
560 relative proportions of the four OC sources in the Svalbard fjords.
561 Nonetheless, both methods showed that the plant-derived OC fraction contributed
562 minimally compared to dominant sources such as petrogenic and marine OC. However,
563 soil-derived OC contributions were higher in the middle (1161MUC) and outer
564 (1159MUC) cores and than in the innermost core (1058MUC), suggesting an additional
565 input likely associated with surface runoff. This is supported by the presence of EM3 in
566 core 1161MUC (Fig. 6B), indicative of significant input of both fine and coarse particles,
567 a feature not observed in the other two cores. Given that core 1161MUC is situated closer
568 to the Byelva River (Fig. 1), the occurrence of EM3 at this site likely reflects the localized
569 influence of surface runoff. This runoff facilitates the transport of terrestrial material,
570 especially soil-derived OC, into the fjord via riverine discharge from the adjacent
571 catchment. This mechanism is consistent with previous studies, which have shown that
572 surface runoff significantly influences the biogeochemical composition of particulate and
573 dissolved matter in Kongsfjorden (e.g., Hop et al., 2002; Svendsen et al., 2002). These
574 inputs are known to deliver high loads of suspended sediments, nutrients, and terrigenous
575 OC, especially during the melt season when hydrological connectivity between the land

and fjord is enhanced. The proximity of core 1161MUC to the Byelva River mouth therefore increases its susceptibility to these runoff-derived materials, which can be subsequently advected toward the outer fjord.

5.5 Potential future implication on carbon dynamics

The bulk OC AR was 0.47 ± 0.06 g/cm²/yr at the middle site (core 1161MUC), higher than the outermost site (core 1159MUC), which had a value of 0.26 ± 0.03 g/cm²/yr (data not shown). The ARs of the four OC sources, determined by both Methods 1 and 2, are presented in Fig. 10. For core 1161MUC, petrogenic OC ARs were similar between Method 1 (0.18 ± 0.03 g/cm²/yr) and Method 2 (0.18 ± 0.02 g/cm²/yr). Among biogenic sources, marine OC had the highest ARs (0.15 ± 0.03 g/cm²/yr for Method 1; 0.17 ± 0.03 g/cm²/yr for Method 2), two to four times higher than soil-derived OC and 20–70 times higher than plant-derived OC. Similarly, for core 1159MUC, petrogenic OC ARs were consistent across both methods (0.05 ± 0.01 g/cm²/yr), with marine OC showing the highest biogenic ARs (0.05 ± 0.01 g/cm²/yr for Method 1; 0.06 ± 0.01 g/cm²/yr for Method 2), exceeding those of soil-derived and plant-derived OC.

For all petrogenic and biogenic OC sources, ARs were higher at the middle site (core 1161MUC) than at the outermost site (core 1159MUC) (Fig. 10). This spatial difference likely reflects the middle site's closer proximity to glacial and fluvial sediment inputs, including the tidewater glaciers (e.g., Kronebreen and Kongsbreen) and the Bayelva River near Ny-Ålesund. Its location may have facilitated more efficient delivery and deposition of sediments and associated OC, resulting in higher ARs. Notably, marine OC ARs at core 1161MUC showed an increasing trend since approximately the 1970s, while petrogenic OC ARs decreased over the same period. In contrast, no clear temporal trends were observed in either petrogenic or marine OC ARs at the outermost site (Fig. S11). This increase in marine OC ARs at the middle site (Fig. 11A) coincides with a shift in sediment composition, characterized by increasing relative abundances of EM1b (Fig. 11B), suggesting intensified meltwater discharge from marine-terminating glaciers. This discharge was likely driven by increased AW inflow, which enhanced basal melting of tidewatr glaciers. Being situated closer to these glaciers, the middle site appears more sensitive to variability in AW inflow. Since increased AW inflow to fjords reduces sea ice cover and delivers nutrients that enhance marine productivity, this process supports greater marine OC burial. In contrast, the outermost site, under more stable AW influence, exhibited relatively consistent marine OC burial over time. Additionally, its lower SRs, a

consequence of its greater distance from the glacier front, may obscure short-term variations in OC deposition. Overall, the differing trends in marine OC ARs between the middle and outermost sites likely reflect differences in hydrographic and sedimentary dynamics, with the middle site more responsive to glacial and oceanographic variability associated with AW inflow.

The rise in marine OC ARs coincides with broader climatic and environmental changes in the Svalbard region. Since the 1970s, surface air temperatures in Ny-Ålesund have increased at a rate four times faster than the global average from 1975 to 2014 (Fig. 11C, Wei et al., 2016). Concurrently, the Barents Sea summer sea ice extent has declined rapidly (Fig. 11D, NSIDC; National Snow and Ice Data Center, http://nsidc.org/data/seaice_index), and the Blomstrandbreen glacier has experienced significant retreat (Fig. 11D, Burton et al., 2016). These changes suggest a strong link between climate warming and shifts in Kongsfjorden's carbon dynamics. Notably, during the same period, integrated temperatures (50 to 300 m water depth) from the transect across 78°N, in the core of the WSC in western Svalbard, also showed an increasing trend (Fig. 11C, Tesi et al., 2021). This suggests a connection between the observed warming of AW and broader regional climatic and environmental changes. Longer-term environmental reconstructions support this connection, with studies reporting increased AW inflow and associated productivity in Kongsfjorden in the early 20th century (Husum et al., 2019; Tesi et al., 2021). Ingrosso et al. (2025) also documented rapid greening of western Svalbard during the same period, which they attributed to extremely low sea ice extent, driven primarily by the strong advection of warm AW into Arctic fjords. This historical context highlights the likely influence of enhanced AW inflow on the rise in marine OC ARs recorded at the middle site (core 1161MUC) since the 1970s, with increased marine productivity and OC burial contributing to this rise while driving the concurrent decline in petrogenic OC ARs.

6. Conclusions

In this study, we investigated three multicores collected from Kongsfjorden, Svalbard, to explore the spatial and temporal dynamics of sedimentary OC over recent centuries. Bulk parameter analyses indicate that Kongsfjorden was the primary source of OC in the sediments, with minor contributions from Krossfjorden. Additionally, a substantial amount of old OC, likely derived from petrogenic and soil sources, was present in the sedimentary OC in Kongsfjorden. To estimate the relative proportions of

OC sources, we applied a four-source apportionment approach based on $\Delta^{14}C_{org}$, $\delta^{13}C_{org}$, and lignin parameters, including the (Ad/Al)v ratio and lignin phenol concentrations, using MC analysis. Our results revealed that petrogenic OC fractions were highest at the innermost site, while marine OC fractions dominated at the outermost site. The plant-derived OC fraction contributed minimally compared to petrogenic and marine OC, while soil-derived OC was more substantial at the middle and outermost sites, suggesting enhanced input from surface runoff. For all OC sources, ARs were higher at the middle site than at the outermost site. Notably, marine OC ARs at the middle site showed an increasing trend since approximately the 1970s, likely reflecting enhanced AW inflow, which boosted marine productivity and OC burial. These findings underscore the significant role of AW inflow in reshaping carbon dynamics in Svalbard fjords over the past few decades and highlight the sensitivity of Arctic fjords to climate shifts. More importantly, our study suggests that the marked increase in AW inflow to Kongsfjorden during the 20th century likely occurred in two distinct phases, around the early 1900s and the 1970s. This pattern reflects a two-step process driven by complex and not yet fully understood mechanisms. To better constrain the timing, drivers, and consequences of AW variability, we emphasize the need for future research that integrates high-resolution climate modeling with sediment core records from Svalbard. Such an integrated approach will be essential for improving projections of climate and carbon cycle feedbacks in the rapidly warming Arctic. Given their role as critical OC reservoirs, Arctic fjords may function as both sources and sinks of carbon in a warming climate, emphasizing the need for further research to assess the long-term consequences of climate-induced changes on regional carbon cycling.

Data availability

All the primary data related to this article are available online at Korea Polar Data Center (http://dx.doi.org/doi:10.22663/KOPRI-KPDC-00002831) or upon request to the corresponding author (Jung-Hyun Kim, jhkim123@kopri.re.kr).

Supplement

The supplementary material related to this article is published together with the article.

Author contributions

D.K. and J.-H.K. designed the study, interpreted the majority of the data, and wrote the manuscript. Y.K.A., M.F., and S.I.N. contributed to sample acquisition. D.K. conducted the biomarker analyses, while Y.K.A. performed the grain size analyses and the end-member modeling. All authors commented on the manuscript and contributed to its revision.

Competing interest

The authors declare that they have no conflict of interest.

Acknowledgements

We sincerely thank the two anonymous reviewers for their insightful and constructive comments, which have significantly improved the quality of the manuscript. We thank the captains and crews of R/V *Helmer Hanssen* for their support at sea during sediment core retrievals. We also extend our gratitude to Y. Son and Y. Joe for their analytical assistance in the laboratory at KOPRI.

Financial support

This study was fully supported by grants from the National Research Foundation of Korea (NRF), funded by the Ministry of Science and ICT (RS-2025-24683148; KOPRI-PN25010).

References

Ahn, Y., Joe, Y. J., Jang, K., Kim, J.-H., Son, Y. J., Forwick, M., Hong, S., Nam, S.-I.: Post-glaciation depositional changes in Wijdefjorden, northern Svalbard, using grain-size end-member modelling. Mar. Geol., 472, 107306, https://doi.org/10.1016/j.margeo.2024.107306, 2024.

Appleby, P. G.: Dating recent sediments by 210 Pb: problems and solutions. Seminar on Dating of sediments and determination of sedimentation rate, pp p. 7–24, https://inis.iaea.org/records/vtsmx-fvz88, 1998.

Appleby, P. G., Oldfield, F.: The calculation of lead-210 dates assuming a constant rate of supply of unsupported ^{210}Pb to the sediment. Catena, 5, 1–8, https://doi.org/10.1016/S0341-8162(78)80002-2, 1978.

Årthun, M., Eldevik, T., Smedsrud, L., Skagseth, O., Ingvaldsen, R.: Quantifying the influence of Atlantic heat on Barents Sea ice variability and retreat, J. Clim., 25, 4736–4743, http://doi.org/10.1175/JCLI-D-11-00466.1, 2012.

Bianchi, T. S., Cui, X., Blair, N. E., Burdige, D. J., Eglinton, T. I., Galy, V.: Centers of organic carbon burial and oxidation at the land-ocean interface, Org. Geochem., 115, 138–155, https://doi.org/10.1016/j.orggeochem.2017.09.008, 2017.

Bianchi, T. S., Cui, X., Blair, N. E.: Fjords as aquatic critical zones (ACZs), Earth Sci. Rev., 203, 103145, https://doi.org/10.1016/j.earscirev.2020.103145, 2020.

Blair, N. E., and Aller, R. C.: The fate of terrestrial organic carbon in the marine environment. Annu. Rev. Mar. Sci., 4, 401–423, https://doi.org/10.1146/annurev-marine-120709-142717, 2012.

Brogi, S. R., Jung, J. Y., Ha, S.-Y., and Hur, J.: Seasonal differences in dissolved organic matter properties and sources in an Arctic fjord: Implications for future conditions, Sci. Total Environ., 694, 133740, https://doi.org/10.1016/j.scitotenv.2019.133740, 2019.

Burton, D. J., Dowdeswell, J. A., Hogan, K. A., Noormets, R.: Marginal fluctuations of a Svalbard surge-type tidewater glacier, Blomstrandbreen, since the Little Ice Age: A record of three surges, Arctic, Antarctic, and Alpine Research, 48, 411–426, http://doi.org/10.1657/AAAR0014-094, 2016.

Cantoni, C., Hopwood, M. J.,Clarke, J. S., Chiggiato, J.,Achterberg, E. P., Cozzi, S.: Glacial drivers of marinebiogeochemistry indicate a future shiftto more corrosive conditions in anArctic fjord, J. Geophys. Res. Biogeosci., 125, e2020JG005633, https://doi.org/10.1029/2020JG005633, 2020.

Choudhary, S., Neelavanan, K., Saalim, S. M.: Microplastics in the surface sediments of Krossfjord-Kongsfjord system, Svalbard, Arctic, Mar. Pollut. Bull., 176, 113452, http://doi.org/10.1016/j.marpolbul.2022.113452, 2022.

Cottier, F. R., Nilsen, F., Inall, M. E., Gerland, S., Tverberg, V., Svendsen, H.: Wintertime warming of an Arctic shelf in response to large-scale atmospheric circulation, Geophys. Res. Lett., 34, L10607, http://doi.org/10.1029/2007GL029948, 2007.

D'Angelo, A., Giglio, F., Miserocchi, S., Sanchez-Vidal, A., Aliani, S., Tesi, T.: Multi-year particle fluxes in Kongsfjorden, Svalbard, Biogeosciences, 15, 5343–5363, https://doi.org/10.5194/bg-15-5343-2018, 2018.

742 Dahlke, F. T., Wohlrab, S., Butzin, M., Pörtner, H.-O.: Thermal bottlenecks in the life
743 cycle define climate vulnerability of fish, Sciences, 369, 65–70,
744 http://doi.org/10.1126/science.aaz3658, 2020.
745 Dallmann, W. K., Elvevold, S.: Bedrock geology. Geoscience Atlas of Svalbard, Re-port
746 Series 148, Norsk Polarinstitutt, Tromsø, pp.133–173,
747 http://hdl.handle.net/11250/2580810, 2015.
748 De Rovere, F., Langone, L., Schroeder, K., Miserocchi, S., Giglio, F., Aliani, S., and
749 Chiggiato, J.: Water masses variability in inner Kongsfjorden (Svalbard) during
750 2010–2020, Front. Mar. Sci., 9, 741075,
751 https://doi.org/10.3389/fmars.2022.741075, 2022.
752 Elverhøi, A., Liestøl, O. and Nagy, J.: Glacial erosion, sedimentation and microfauna in
753 the inner part of Kongsfjorden, Spitsbergen, Norsk Polarinstitutt Skrifter, 172, 33–
754 58, http://core.ac.uk/reader/30910780#page=35, 1980.
755 Forwick, M., Vorren, T. O.: Late Weichselian and Holocene sedimentary environments
756 and ice rafting in Isfjorden, Spitsbergen, Palaeogeogr. Palaeoclimatol. Palaeoecol.,
757 280, 258–274, http://doi.org/10.1016/j.palaeo.2009.06.026, 2009.
758 Friedlingstein, P., et al.: Global carbon budget 2020, Earth Syst. Sci. Data, 12, 3269–3340,
759 http://doi.org/10.5194/essd-12-3269-2020, 2020.
760 Gealy, E. L.: Saturated bulk density, grain density, and porosity of sediment cores from
761 the western equatorial Pacific: Leg 7, Glomar Challenger. Initial Reports of the
762 Deep Sea Drilling Project, 7, 1081–1104, 1971.
763 Goñi, M. A., and Hedges, J. I.: Lignin dimers: structures, distribution, and potential
764 geochemical applications, Geochim. Cosmochim. Acta, 56, 4025–4043,
765 https://doi.org/10.1016/0016-7037(92)90014-A, 1992.
766 Goñi, M. A., and Hedges, J. I.: Sources and reactivities of marine-derived organic matter
767 in coastal sediments as determined by alkaline CuO oxidation, Geochim.
768 Cosmochim. Acta, 59, 2965–2981, https://doi.org/10.1016/0016-7037(95)00188-3,
769 1995.
770 Goñi, M. A., Yunker, M. B., MacDonald, R. W., and Eglinton, T. I.: Distribution and
771 sources of organic biomarkers in arctic sediments from the Mackenzie River and
772 Beaufort Shelf, Mar. Chem., 71, 23–51, https://doi.org/10.1016/S0304-
773 4203(00)00037-2, 2000.
774 Goñi, M. A., Yunker, M. B., MacDonald, R. W., and Eglinton, T. I.: The supply and
775 preservation of ancient and modern components of organic carbon in the Canadian

776 Beaufort Shelf of the Arctic Ocean, Mar. Chem., 93, 53–73,
777 https://doi.org/10.1016/j.marchem.2004.08.001, 2005.
778 Hamilton, E. L.1971 Elastic properties of marine sediments, J. Geophys. Res., 76, 293–
779 635, https://doi.org/10.1190/1.1440168, 1971.
780 Hass, H. C.: A method to reduce the influence of ice-rafted debris on a grain size record
781 from northern Fram Strait, Arctic Ocean, Polar Res., 21, 299–306,
782 http://doi.org/10.1111/j.1751-8369.2002.tb00084.x, 2002.
783 Hedges, J. I., and Ertel, J. R.: Characterization of lignin by gas capillary chromatography
784 of cupric oxide oxidation products, Anal. Chem., 54, 174–178,
785 https://doi.org/10.1021/ac00239a007, 1982.
786 Hedges, J. I., and Mann, D. C.: The characterization of plant tissues by their lignin
787 oxidation products, Geochim. Cosmochim. Acta, 43, 1803–1807,
788 https://doi.org/10.1016/0016-7037(79)90028-0, 1979.
789 Hop, H., et al.: The marine ecosystem of Kongsfjorden, Svalbard, Polar Res., 21, pp.167-
790 208, http://doi.org/10.1007/978-3-319-46425-1_1, 2002.
791 Houel, S., Louchouarn, P., Lucotte, M., Canuel, R., and Ghaleb, B.: Translocation of soil
792 organic matter following reservoir impoundment in boreal systems: Implications
793 for in situ productivity, Limnol. Oceanogra., 51, 1497–1513,
794 https://doi.org/10.4319/lo.2006.51.3.1497, 2006.
795 Husum, K., et al.: The marine sedimentary environments of Kongsfjorden, Svalbard: An
796 archive of polar environmental change, Polar Res., 38, 3380,
797 https://doi.org/10.33265/polar.v38.3380, 2019.
798 Ingrosso, G., Ceccarelli, C., Giglio, F., Giordano, P., Hefter, J., Langone, L., Miserocchi,
799 S., Mollenhauer, G., Nogarotto, A., Sabino, M., Tesi, T.: Greening of Svalbard in
800 the twentieth century driven by sea ice loss and glaciers retreat, Commun. Earth
801 Environ., 6, 30, http://doi.org/10.1038/s43247-025-01994-y, 2025.
802 Ito, H., and S. Kudoh,: Characteristics of water in Kongsfjorden, Svalbard, Proc. NIPR
803 Symp. Polar Meteorol. Glaciol., 11, 211–232, 1997.
804 Jernas, P., et al.: Annual changes in Arctic fjord environment and modern benthic
805 foraminiferal fauna: Evidence from Kongsfjorden, Svalbard, Global Planet. Change,
806 163, 119–140, 2018.
807 Jordà-Molina, È., Renaud, P. E., Silberberger, M. J., Sen, A., Bluhm, B. A., Carroll, M.
808 L., Ambrose Jr., W. G., Cottier, F., Reiss, H.: Seafloor warm water temperature
809 anomalies impact benthic macrofauna communities of a high-Arctic cold-water

fjord. Mar. Envrion. Res., 189. 106046, http://doi.org/10.1016/j.marenvres.2023.106046, 2023.

Keil, R. G., Tsamakis, E., Fuh, C. B., Giddings, J. C., Hedges, J. I.: Mineralogical and textural controls on the organic composition of coastal marine sediments: Hydrodynamic separation using SPLITT-fractionation, Geochim. Cosmochim. Acta, 58, 879–893, https://doi.org/10.1016/0016-7037(94)90512-6, 1994.

Keil, R. G., Mayer, L. M., Quay, P. D., Richey, J. E., Hedges, J. I.: Loss of organic matter from riverine particles in deltas, Geochim. Cosmochim. Acta, 61, 1507–1511, https://doi.org/10.1016/S0016-7037(97)00044-6, 1997.

Kim, J.-H., Peterse, F., Willmott, V., Klitgaard Kristensen, D., Baas, M., Schouten, S., Sinninghe Damsté, J.S.: Large ancient organic matter contributions to Arctic marine sediments (Svalbard), Limnol. Oceanogr., 56, 1463–1474, http://doi.org/10.4319/1o.2011.56.4.1463, 2011.

Kim, D., Kim, J.-H., Tesi, T., Kang, S., Nogarotto, A., Park, K., Lee, D.-H., Jin, Y.K., Shin, K.-H., Nam, S.-I.: Changes in the burial efficiency and composition of terrestrial organic carbon along the Mackenzie Trough in the Beaufort Sea, Estuar. Coastal Shelf Sci., 275, 107997, https://doi.org/10.1016/j.ecss.2022.107997, 2022.

Kim, D., Kim, J.-H., Ahn, Y., Jang, K., Jung, J. Y., Bae, M., Nam, S.-I.: Large contributions of petrogenic and aged soil-derived organic carbon to Arctic fjord sediments in Svalbard, Sci. Rep., 13, 17935, https://doi.org/10.1038/s41598-023-45141-z, 2023.

Knies, J., Martinez, P.: Organic matter sedimentation in the western Barents Sea region: Terrestrial and marine contribution based on isotopic composition and organic nitrogen content. Nor. J. Geol., 89, 79–89, 2009.

Knies, J., Brookes, S., Schubert, C. J.: Re-assessing the nitrogen signal in continental margin sediments: New insights from the high northern latitudes, Earth Planet. Sci. Lett., 253, 471–484, http://doi.org/10.1016/j.epsl.2006.11.008, 2007.

Krajewska, M., Szymczak-Zyla, M., Tylmann, W., Kowalewska, G.: Climate change impact on primary production and phytoplankton taxonomy in Western Spitsbergen fjords based on pigments in sediments, Global Planet. Change, 189, 103158, http://doi.org/10.1016/j.gloplacha.2020.103158, 2020.

Kumar, V., Tiwari, M., Nagoji, S., Tripathi, S.: Evidence of anomalously low $\delta^{13}C$ of marine organic matter in an Arctic Fjord, Sci. Rep., 6, 36192, http://10.1038/srep36192, 2016.

Lind, S., Ingvaldsen, R. B., Furevik, T.: Arctic warming hotspot in the northern Barents Sea linked to declining sea-ice import, Nat. Clim. Change, 8, 634–639, 2018.

Mayer, L. M.: Surface area control of organic carbon accumulation in continental shelf sediments, Geochim. Cosmochim. Acta, 58, 1271–1284, https://doi.org/10.1016/0016-7037(94)90381-6, 1994.

McGovern, M., Borgå, K., Heimstad, E., Ruus, A., Christensen, G., Evenset, A.: Small Arctic rivers transport legacy contaminants from thawing catchments to coastal areas in Kongsfjorden, Svalbard, Environ. Pollut., 304, 119191, https://doi.org/10.1016/j.envpol.2022.119191, 2022.

Meslard, F., Bourrin, F., Many, G., Kerherve, P.: Suspended particle dynamics and fluxes in an Arctic fjord (Kongsfjorden, Svalbard), Estuar. Coast. Shelf Sci., 204, 212–224, http://doi.org/10.1016/j.ecss.2018.02.020, 2018.

Nam, S.-I.: Late Quaternary glacial history and paleoceanographic reconstructions along the East Greenland continental marine: evidence from high-resolution records of stable isotopes and ice-rafted debris, Rep. Polar Res., 241, pp. 21, https://epic.awi.de/id/eprint/26419/1/BerPolarforsch1997241.pdf, 1997.

Nuth, C., Kohler, J., Konig, M., von Deschwanden, A., Hagen, J. O., Kaab, A., Moholdt, G., Pettersson, R.: Decadal changes from a multi-temporal glacier inventory of Svalbard. The Cryosphere, 7, 1603–1621, http://doi.org/10.5194/tc-7-1603-2013, 2013.

Ó Cofaigh, C., Dowdeswell, J. A.: Laminated sediments in glacimarine environments: diagnostic criteria for their interpretation, Quat. Sci. Rev., 20, 1411–1436, http://doi.org/10.1016/S0277-3791(00)00177-3, 2001.

Otto, A., and Simpson, M. J.: Evaluation of CuO oxidation parameters for determining the source and stage of lignin degradation in soil, Biogeochem., 80, 121–142, https://doi.org/10.1007/s10533-006-9014-x, 2006.

Pempkowiak, J.: Limitation of lignin derivatives as biomarkers of land derived organic matter in the coastal marine sediments, Oceanologia, 62, 374–386, http://doi.org/10.1016/j.oceano.2020.04.004, 2020.

Polyakov, I. V., Pnyushkov, A. V., Alkire, M. B., Ashik, I. M., Baumann, T. M., Carmack, E. C., Goszczko, I., Guthrie, J., Ivanov, V. V., Kanzow, T., Krishfield, R., Kwok, R., Sundfjord, A., Morison, J., Remember, R., Yulin, A.: Greater role for Atlantic inflows on sea-ice loss in the Eurasian Basin of the Arctic Ocean, Science, 356, 285–291, 2017.

878 Prahl, F. G., Ertel, J. R., Goñi, M. A., Sparrow, M. A., Eversmeyer, B.: Terrestrial organic
879 carbon contributions to sediments on the Washington margin, Geochim.
880 Cosmochim. Acta, 58, 3035–3048, https://doi.org/10.1016/0016-7037(94)90177-5,
881 1994.
882 Pramanik, A., Kohler, J., Lindback, K., How, P., Van Pelt, W., Liston, G., Schuler, T. V.:
883 Hydrology and runoff routing of glacierized drainage basins in the Kongsfjord area,
884 northwest Svalbard, The Cryosphere, http://doi.org/10.5174/tc-2020-197, 2020.
885 Rantanen, M., Karpechko, A. Y., Lipponen, A., Nordling, K., Hyvärinen, O., Ruosteenoja,
886 K., Räisänen, J.: The Arctic has warmed nearly four times faster than the globe
887 since 1979, Commun. Earth Environ., 3, 168, https://doi.org/10.1038/s43247-022-
888 00498-3, 2022.
889 Saloranta, T. M., Svendsen, H.: Across the Arctic front west of Spitsbergen: high-
890 resolution CTD sections from 1998–2000, Polar Research, 20, 177–184,
891 http://doi.org/10.3402/polar.v20i2.6515, 2001.
892 Schauer, U., Fahrbach, E., Osterhus, S., Rohardt, G.: Arctic warming through the Fram
893 Strait: Oceanic heat transport from 3 years of measurements, J. Geophys. Res.
894 Oceans, 109, C06026, https://doi.org/10.1029/2003JC001823, 2004.
895 Singh, D. S., Dubey, C. A., Kumar, D., Vishawakarma, B., Singh, A. K., Tripathi, A.,
896 Sharma, R.: Monsoon variability and major climatic events between 25 and 0.05 ka
897 BP using sedimentary parameters in the Gangotri glacier region, Garhwal Himalaya,
898 India. Quater. Inter., 507, 148–155, https://doi.org/10.1016/j.quaint.2019.06.024,
899 2019.
900 Skogseth, R., Asplin, L., Budgell, W. P., Eldevik, T., Gerland, S., Haugan, P., Zamelczyk,
901 K.: Variability and decadal trends in the Isfjorden (Svalbard) ocean climate and
902 circulation – An indicator for climate change in the European Arctic, Progr.
903 Oceanogr., 187, 102394, https://doi.org/10.1016/j.pocean.2020.102394, 2020.
904 Smith, R. W., Bianchi, T. S., Allison, M., Savage, C., Galy, V.: High rates of organic
905 carbon burial in fjord sediments globally, Nat. Geosci., 8, 450–453,
906 http://doi.org/10.1038/NGEO2421, 2015.
907 Stein, R., and MacDonald, R. W.: The organic carbon cycle in the Arctic Ocean, Springer.
908 https://doi.org/10.1007/978-3-642-18912-8, 2004.
909 Stuiver, M., and Polach, H. A.: Discussion: Reporting of 14C data. Radiocarbon, 19, 355–
910 363, https://doi.org/10.1017/S0033822200003672, 1977.

911 Svendsen, H., Beszczynska-Møller, A., Hagen, J. O., Lefauconnier, B., Tverberg, V.,
912 Gerland, S., Ørbæk, J. B.: The physical environment of Kongsfjorden–Krossfjorden,
913 an Arctic fjord system in Svalbard, Polar Res., 21, 133–166,
914 https://doi.org/10.3402/polar.v21i1.6479, 2002.
915 Tesi, T., Muschitiello, F., Smittenber, R. H., Jakobsson, M., Vonk, J. E., Hill, P.,
916 Andersson, A., Kirchner, N., Noormets, R., Dudarev, O., Semiletov, I., Gustafsson,
917 Ö.: Massive remobilization of permafrost carbon during past-glacial warming, Nat.
918 Commun., 7, 13653, http://doi.org/10.1038/ncomms13653, 2016.
919 Tesi, T., Muschitiello, F., Mollenhauer, G., Miserocchi, S., Langone, L., Ceccarelli, C.,
920 Panieri, G., Chiggiato, J., Nogarotto, A., Hefter, J., Ingrosso, G., Giglio, F.,
921 Giordano, P., Capotondi, L.: Rapid atlantification along the Fram Strait at the
922 beginning of the 20th century, Sci. Advances, 7, eabj2946,
923 http://doi.org/10.1126/sciadv.abj2946, 2021.
924 Torsvik, T., Albretsen, J., Sundfjord, A., Kohler, J., Sandvik, A. D., Skarohamar, J.,
925 Lindback, K., Everett, A.: Impact of tidewater glacier retreat on the fjord system:
926 Modeling present and future circulation in Kongsfjorden, Svalbard, Estuar. Coast.
927 Shelf Sci., 220, 152–165, http://doi.org/10.1016/j.ecss.2019.02.005, 2019.
928 Tverberg, V., Skogseth, R., Cottier, F., Sundfjord, A., Walczowski, W., Inall, M. E., Falck,
929 E., Pavlova, O., Nilsen, F.: The Kongsfjorden transect: seasonal and inter-annual
930 variability in hydrography, The Ecosystem of Kongsfjorden, Svalbard, 49–104,
931 http://doi.org/10.1007/978-3-319-46425-1_3, 2019.
932 van Hateren, J. A., Prins, M. A., van Balen, R. T.: On the genetically meaningful
933 decomposition of grain-size distributions: A comparison of different end-member
934 modelling algorithms, Sediment. Geol., 375, 49–71,
935 http://doi.org/10.1016/j.sedgeo.2017.12.003, 2018.
936 Vorren, T. O., Hald, M., Thomsen, E.: Quaternary sediments and environments on the
937 continental shelf off northern Norway, Mar. Geol., 57, 229–257,
938 http://doi.org/10.1016/0025-3227(84)90201-9, 1984.
939 Wei, T., Ding, M., Wu, B., Lu, C., and Wang, S.: Variations in temperature-related
940 extreme events (1975–2014) in Ny-Ålesund, Svalbard, Atmos. Sci. Lett., 17, 102–
941 108, https://doi.org/10.1002/asl.632, 2016.
942 Winkelmann, D., Knies, J.: Recent distribution and accumulation of organic carbon on
943 the continental marine west off Spitsbergen, Geochem. Geophys. Geosyst., 6,
944 Q09012, http://doi.org/10.1029.2005GC000916, 2005.

945 Zaborska, A., Pempkowiak, J., Papucci, C.: Some sediment characteristics and
946 sedimentation rates in an Arctic fjord (Kongsfjorden, Svalbard), Annu. Environ.
947 Prot., 8, pp.79–96, 2006.
948 Zhu, Z.-Y., Wu, Y., Liu, S.-M., Wenger, F., Hu, J., Zhang, J., Yao, P.: Organic carbon
949 flux and particulate organic matter composition in Arctic valley glaciers: Examples
950 from the Bayelva River and adjacent Kongsfjorden, Biogeosciences, 13, 975–987,
951 https://doi.org/10.5194/bg-13-975-2016, 2016.
952 Zonneveld, K. A. F., Versteegh, G. J. M., and de Lange, G. J.: Preservation of organic-
953 walled dinoflagellate cysts in different oxygen regimes: A 10,000 years natural
954 experiment. Mar. Micropaleontol., 29, 393–405, https://doi.org/10.1016/S0377-
955 8398(96)00032-1, 1997.

Figures

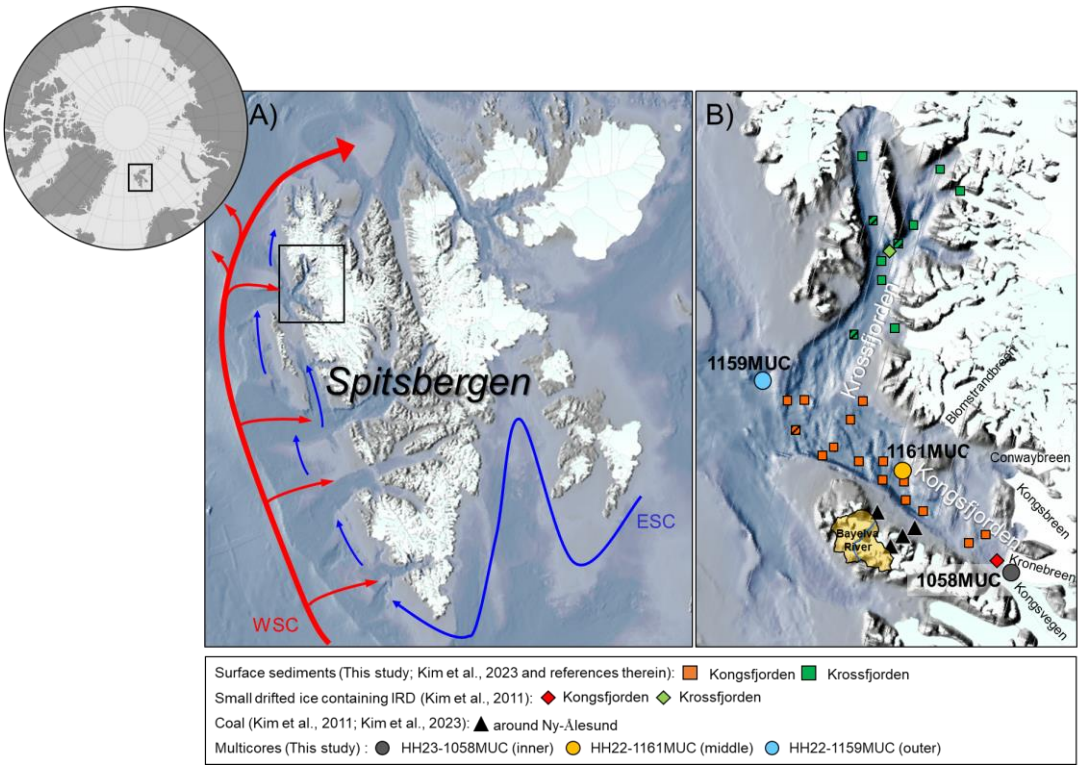

Fig. 1. Map of the study area showing (A) the Svalbard archipelago and (B) the sampling sites in Kongsfjoren and Krossfjorden considered in this study. White land areas indicate present-day glacier coverage. Red and blue arrows indicate the main Atlantic (West Spitsbergen Current, WSC) and Arctic (East Spitsbergen Current, ESC) water currents, respectively. Filled circles represent multicore sampling sites, while filled square, diamond, and triangle symbols indicate surface sediment, small drifted ice containing IRD, and coal sampling sites in Kongsfjorden and Krossfjorden. It should be noted that the surface sediment samples newly analyzed in this study are denoted by hashed square symbols. The map was generated using QGIS v3.14 (https://qgis.org/en/site/forusers/visualchangelog314/) based on IBCAOv4 (https://www.ngdc.noaa.gov/mgg/bathymetry/arctic/).

973

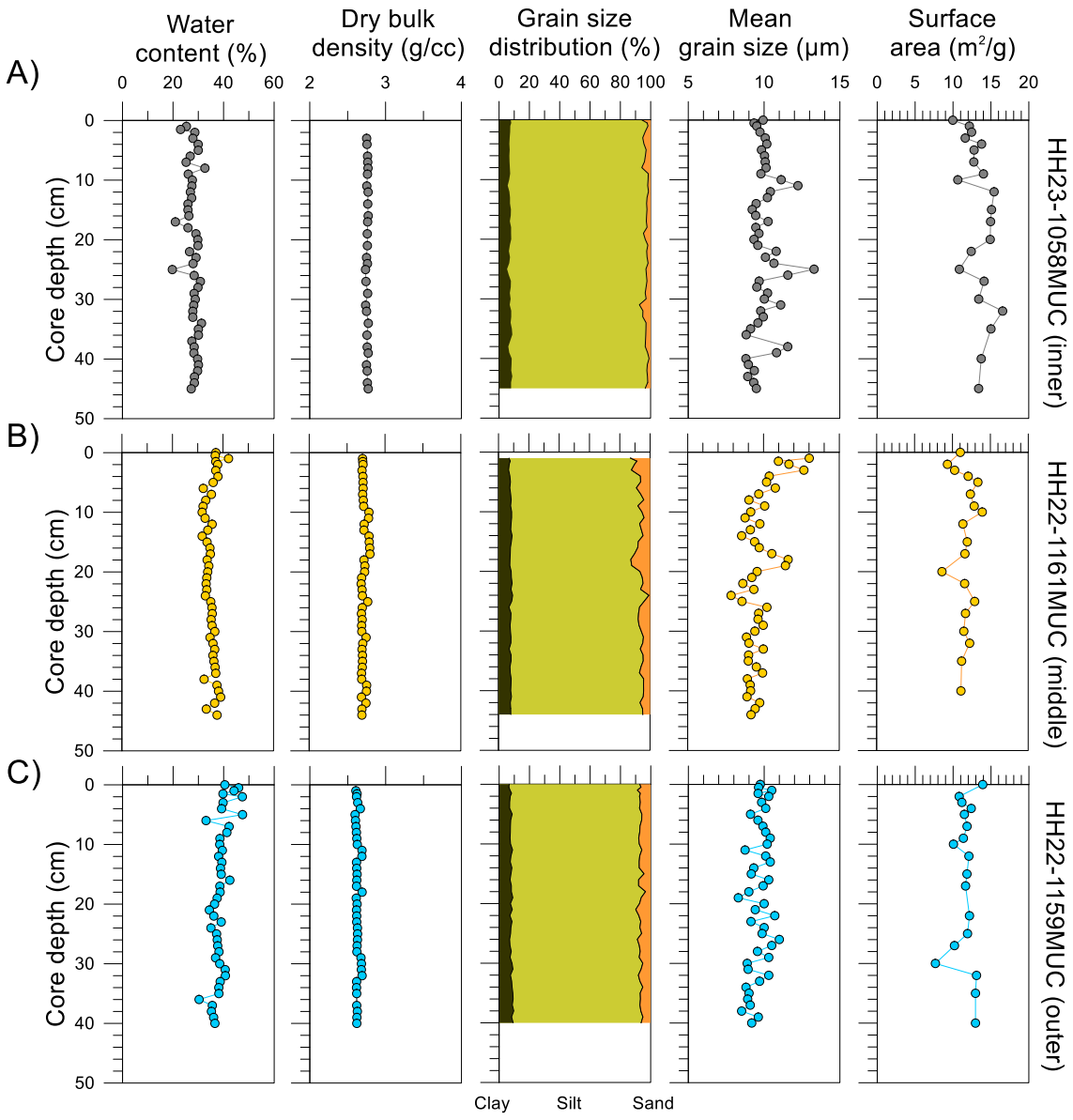

974

975 Fig. 2. Depth profiles of water content (%), dry bulk density (g/cc), grain size distribution
976 (%), mean grain size (μm), and surface area (m^2/g) for the cores (A) HH23-1058MUC,
977 (B) HH22-1161MUC, and (C) HH22-1159MUC.

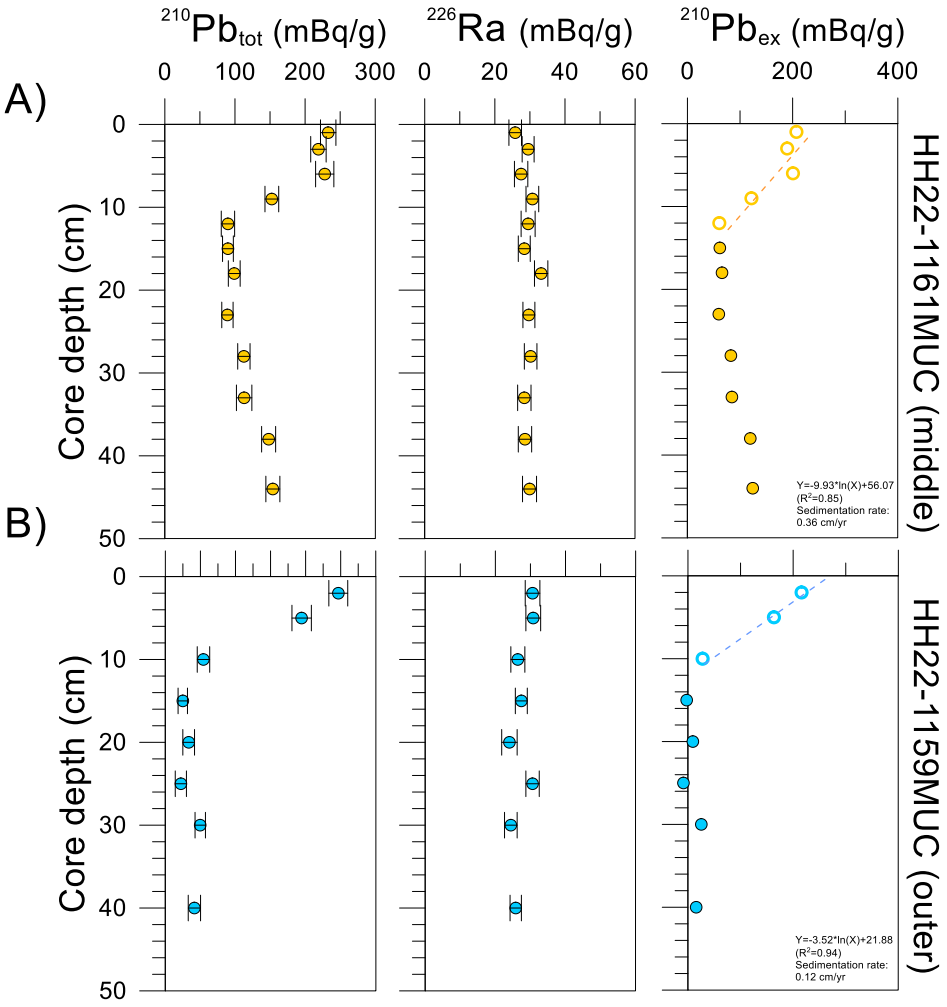

Fig. 3. Depth profiles of $^{210}Pb_{tot}$ (mBq/g), ^{226}Ra (mBq/g), and $^{210}Pb_{ex}$ (mBq/g) for the cores (A) HH22-1161MUC, and (B) HH22-1159MUC. Open circles indicate the data points used in the linear regressions (yellow and blue dotted lines) of the natural log-transformed $^{210}Pb_{ex}$ versus depth, which were applied to estimate sedimentation rates.

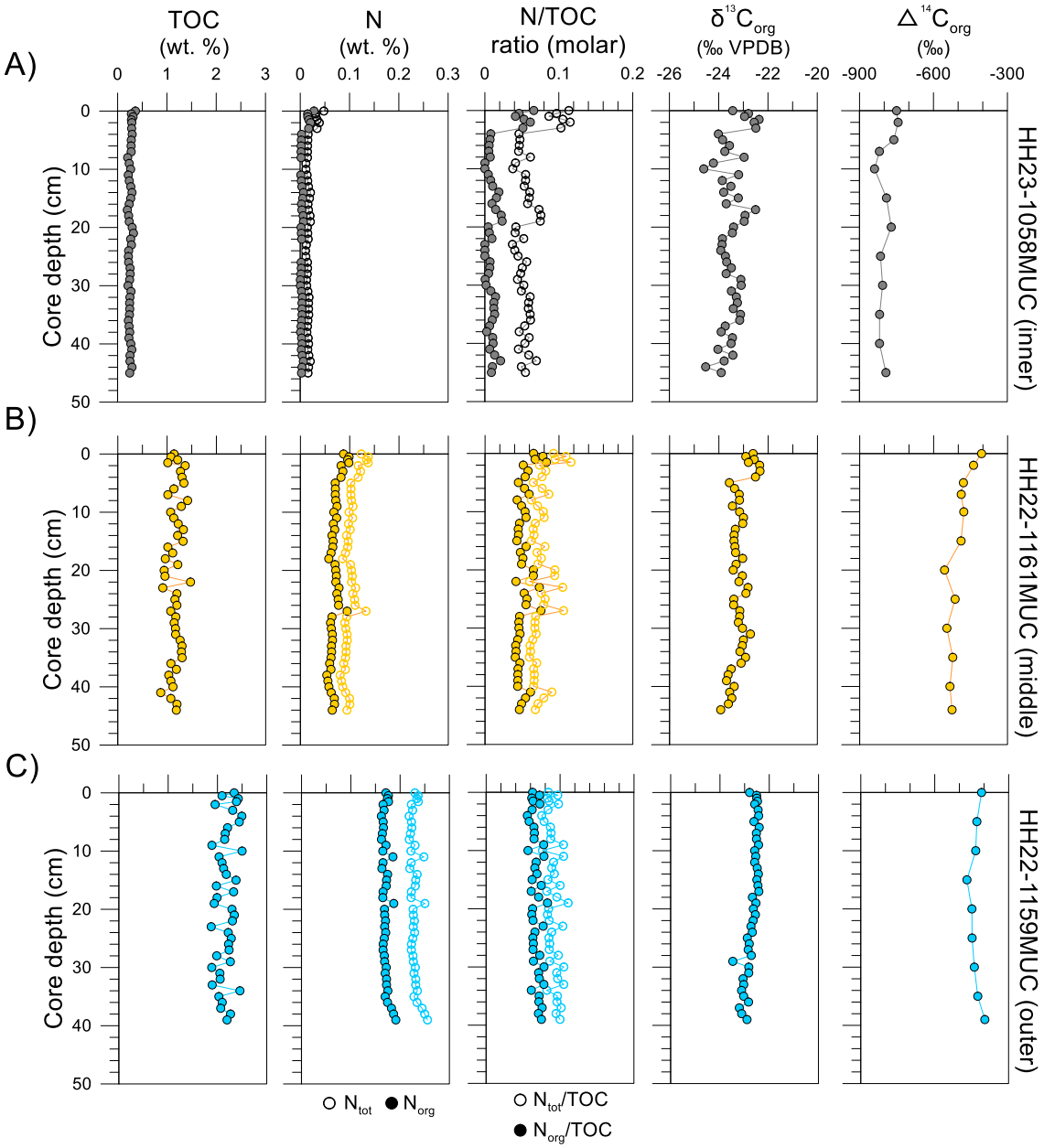

Fig. 4. Depth profiles of TOC (wt. %), N (wt. %), N/TOC ratios (molar), $\delta^{13}C_{org}$ (‰ VPDB), and $\Delta^{14}C_{org}$ (‰) for the cores (A) HH23-1058MUC, (B) HH22-1161MUC, and (C) HH22-1159MUC.

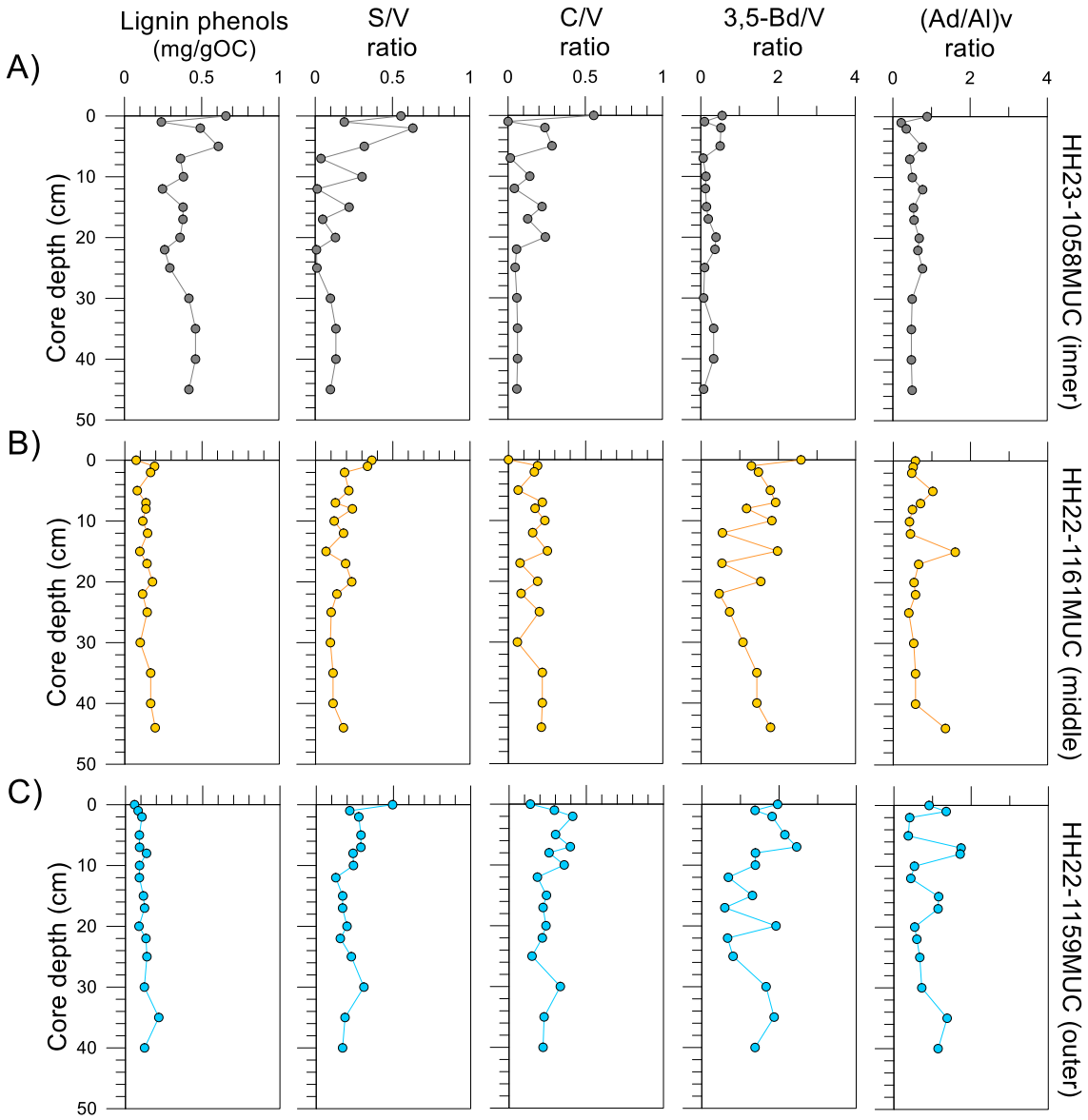

Fig. 5. Depth profiles of lignin phenol concentrations (mg/gOC), and S/V, C/V, 3,5-Bd/V, and (Ad/Al)v ratios for the cores (A) HH23-1058MUC, (B) HH22-1161MUC, and (C) HH22-1159MUC.

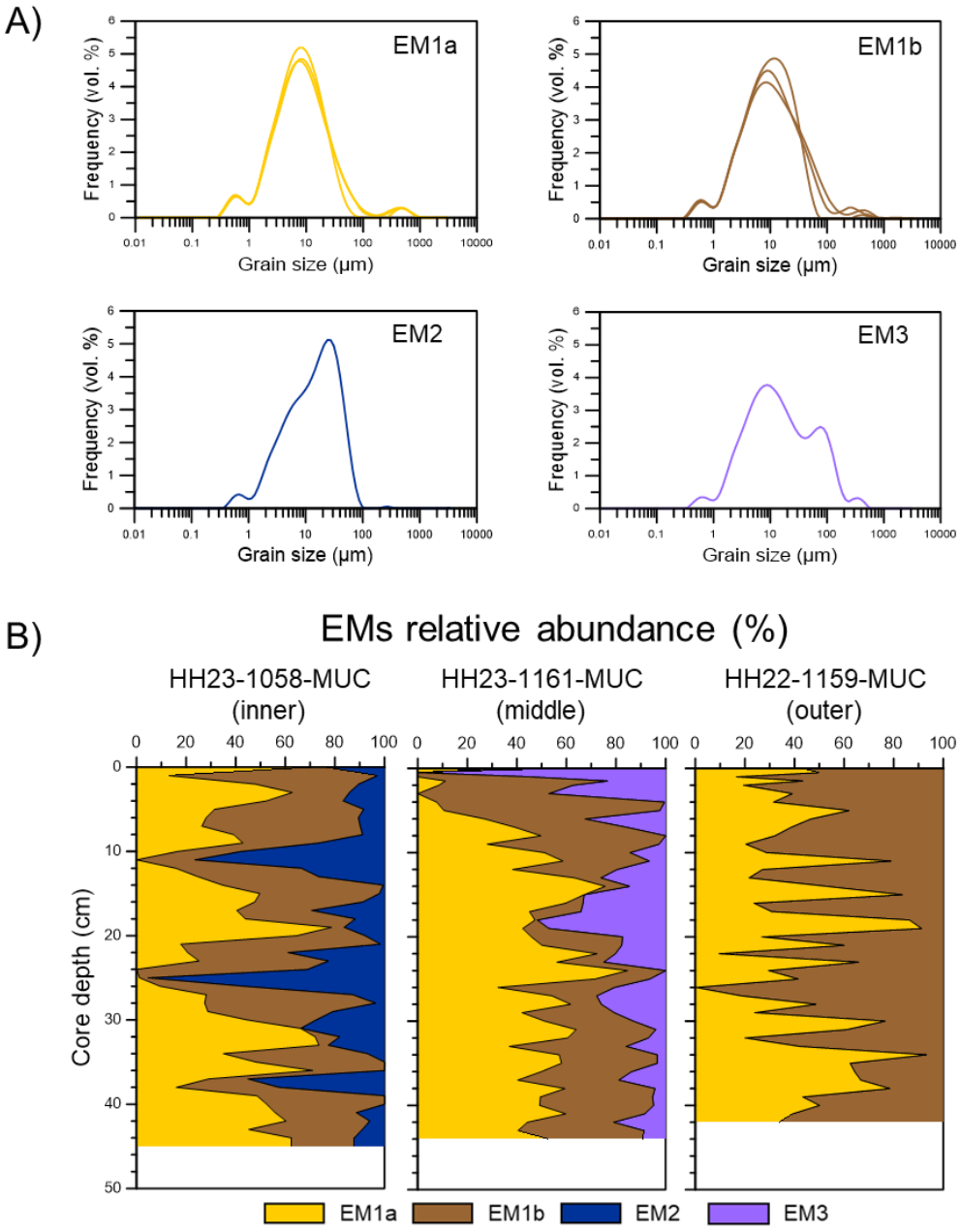

992

993 Fig. 6. (A) Classified grain-size end-member distribution curves from three cores, and (B)
994 depth profiles showing the variation in the relative abundances of grain-size end-members
995 (EM1a, EM1b, EM2, and EM3) in the three cores analyzed in this study.

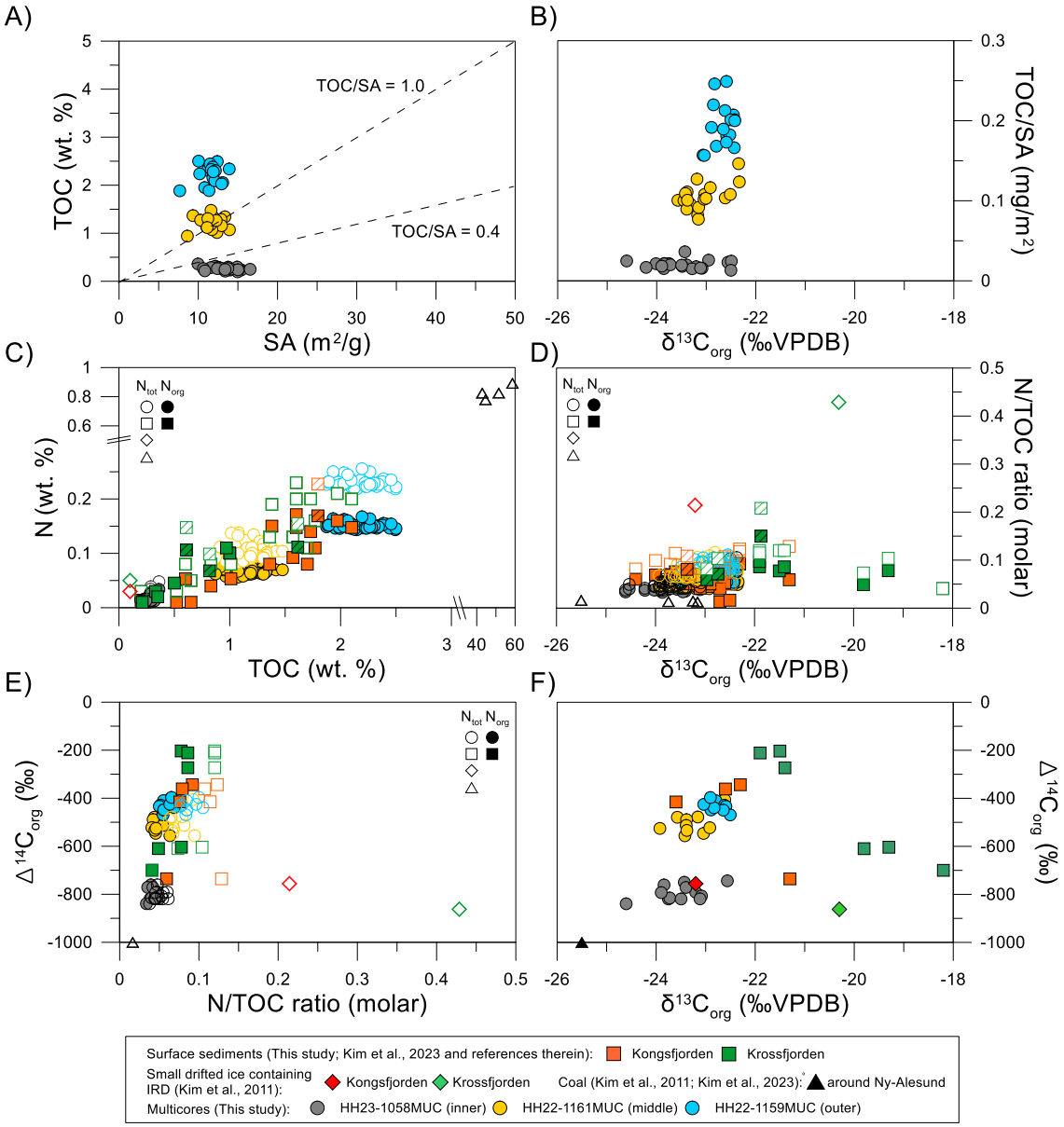

Fig. 7. Scatter plots of (A) SA (m^2/g) versus TOC (wt.%), (B) $\delta^{13}C_{org}$ (‰ VPDB) versus TOC/SA (mg/m^2), (C) TOC (wt.%) versus N_{tot} or N_{org} (wt.%), (D) $\delta^{13}C_{org}$ (‰ VPDB) versus N_{tot}/TOC (molar) ratios or N_{org}/TOC (molar) ratios, (E) N_{tot}/TOC (molar) ratios or N_{org}/TOC (molar) ratios versus $\Delta^{14}C_{org}$ (‰), and (F) $\delta^{13}C_{org}$ (‰ VPDB) versus $\Delta^{14}C_{org}$ (‰) for the three cores, compared with data from small drifted ice containing IRD (Kim et al., 2011), coals (Kim et al., 2011; Kim et al., 2023), and surface sediments (Kim et al., 2023 and this study). Note that the surface sediment samples newly analyzed in this study are denoted by hashed square symbols.

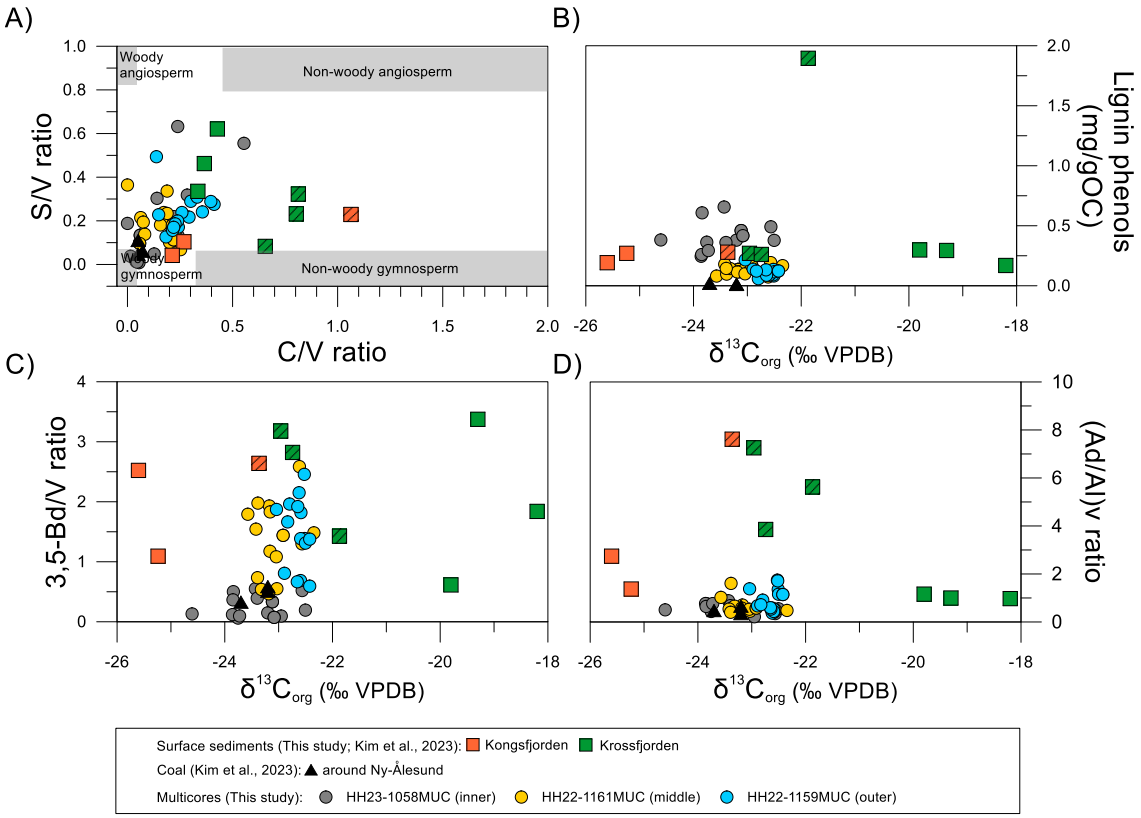

Fig. 8. Scatter plots of (A) C/V ratio versus S/V ratio, including the end-members for different vascular plant tissues (cf. Goñi et al., 2000), (B) $\delta^{13}C_{org}$ (‰ VPDB) versus lignin phenols (mg/gOC), (C) $\delta^{13}C_{org}$ (‰ VPDB) versus 3,5-Bd/V ratio, and (D) $\delta^{13}C_{org}$ (‰ VPDB) versus (Ad/Al)v ratio for the three cores, compared with data from coals (Kim et al., 2023) and surface sediments (Kim et al., 2023 and this study). Note that the surface sediment samples newly analyzed in this study are indicated by hashed square symbols.

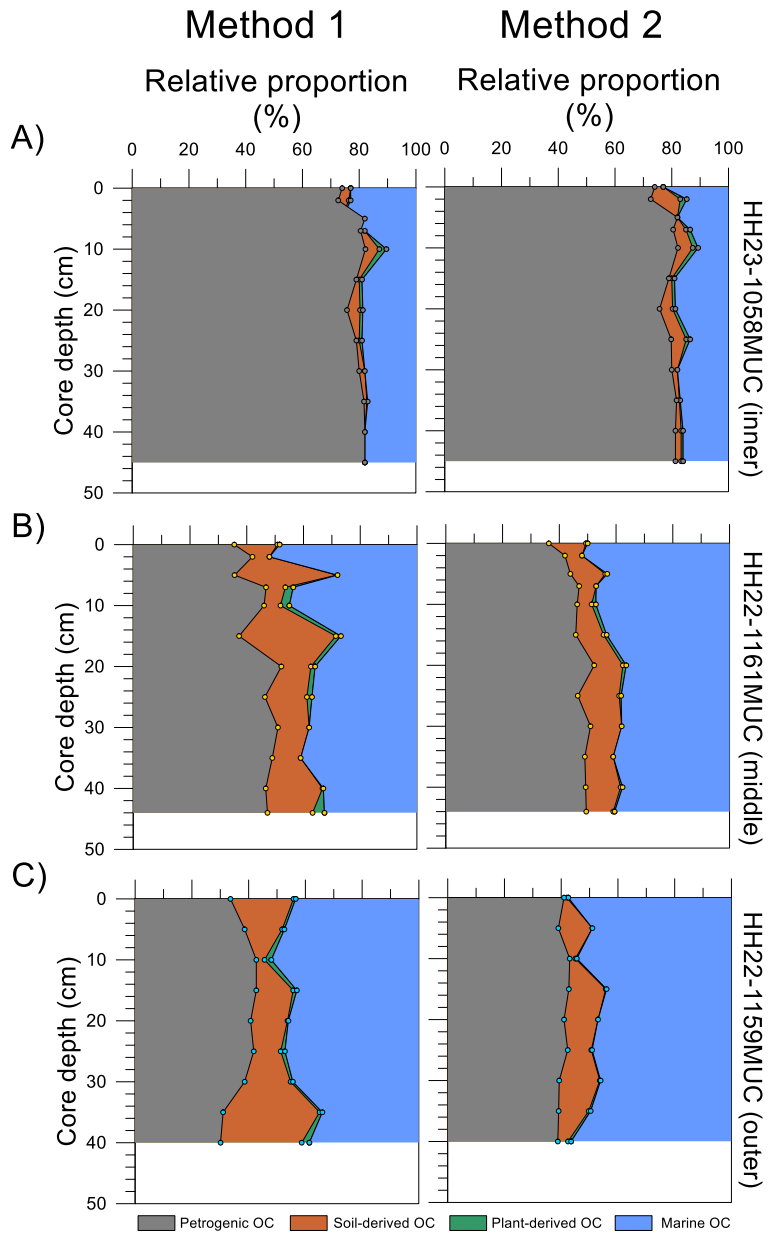

Fig. 9. Depth profiles showing the relative proportions of petrogenic, soil-derived, plant-derived, and marine OC, as determined using Method 1 (based on $\delta^{13}C_{org}$ (‰ VPDB), $\Delta^{14}C_{org}$ (‰), and (Ad/Al)v ratio) and Method 2 (based on $\delta^{13}C_{org}$ (‰ VPDB), $\Delta^{14}C_{org}$ (‰), and lignin phenols (mg/gOC)), for the cores (A) HH23-1058MUC, (B) HH22-1161MUC, and (C) HH22-1159MUC.

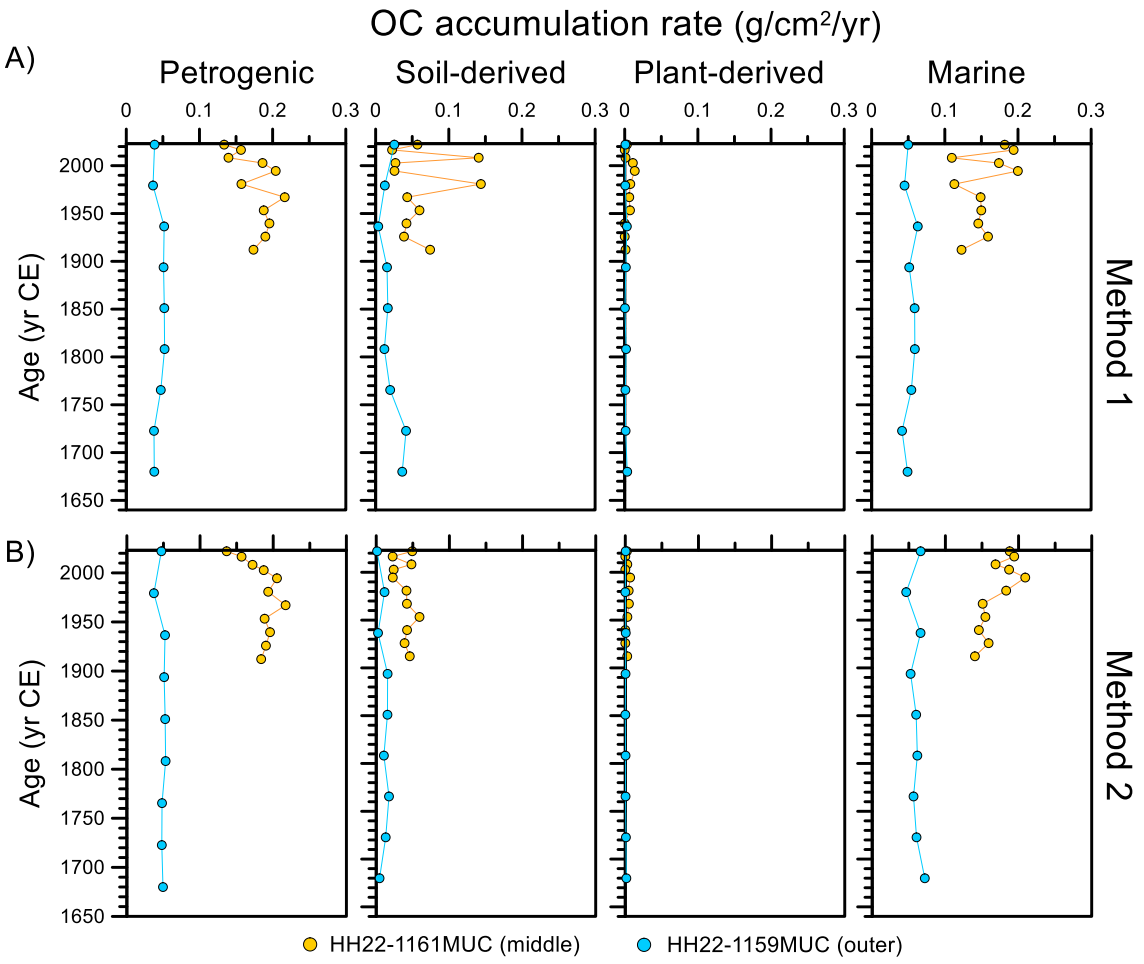

Fig. 10. Age profiles of the accumulation rates (g/cm^2/yr) of petrogenic, soil-derived, plant-derived, and marine OC, as determined using Method 1 (based on $\delta^{13}C_{org}$ (‰ VPDB), $\Delta^{14}C_{org}$ (‰), and (Ad/Al)v ratio) and Method 2 (based on $\delta^{13}C_{org}$ (‰ VPDB), $\Delta^{14}C_{org}$ (‰), and lignin phenols (mg/gOC)), for the cores HH23-1058MUC, HH22-1161MUC, and HH22-1159MUC.

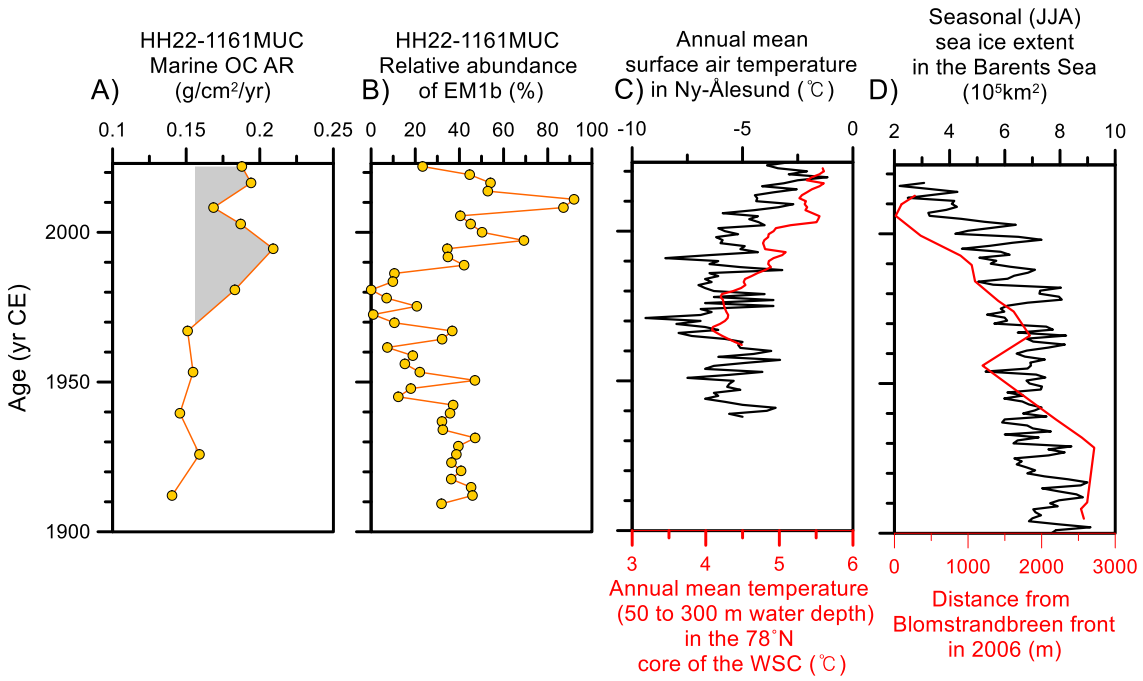

Fig. 11. Age profiles of (A) the accumulation rates of marine OC based on Method 2 for core HH22-1161MUC, (B) the relative abundance (%) of EM1b for core HH22-1161MUC, (C) annual mean surface air temperatures (°C) in Ny-Ålesund (black; data from MOSJ, Environmental monitoring of Svalbard and Jan Mayen) and integrated annual mean temperatures (°C) at 50-300 m water depth in the 78°N core of the West Spitsbergen Current (red; data from MOSJ), and (D) seasonal (JJA) sea ice extent in the Barents Sea (black; data from NSIDC; National Snow and Ice Data Center) and the distance from the Blomstrandbreen front in Kongsfjorden in 2006 (red; data from Burton et al., 2016).